

Numerical simulation of the miscible displacement of radionuclides in a heterogeneous porous medium

C.-H. Bruneau^{*,†}, F. Marpeau[‡] and M. Saad[§]

Mathématiques Appliquées de Bordeaux (MAB), Université Bordeaux 1, 351 Cours de la Libération, 33405 Talence Cedex, France

SUMMARY

The aim of this paper is to model and simulate the displacement of radioactive elements in a saturated heterogeneous porous medium. New schemes are proposed to solve accurately the convection–diffusion–reaction equations including nonlinear terms in the time derivative. Numerical tests show the stability and robustness of these schemes through strong heterogeneities of the medium. Finally the COUPLEX 1 benchmark concerning the far field simulation of a polluted flow by a leak of a nuclear waste disposal is performed and compared with the results available in the literature. Copyright © 2005 John Wiley & Sons, Ltd.

KEY WORDS: convection–diffusion–reaction operators; Darcy’s law; adsorption; heterogeneous porous medium; radionuclide; flux limiting scheme

1. INTRODUCTION

Human activities use the radioactivity in several fields, for instance the production of electricity or medicine. The main attraction of this process is the possibility to produce a large amount of energy. Nevertheless, in all the physical applications of the nuclear fission, the disintegration of a radionuclide always produces other elements, generally radioactive too. These products are useless, but are still dangerous for years. Since they cannot be totally destroyed, the only way to avoid a contamination is to stock these nuclear wastes into some containers that are buried underground. Many studies deal with the safety of this kind of repositories in order to prevent the pollution of the ground by an eventual leak of the con-

*Correspondence to: C.-H. Bruneau, Mathématiques Appliquées de Bordeaux (MAB), Université Bordeaux 1, 351 Cours de la Libération, 33405 Talence Cedex, France.

†E-mail: bruneau@math.u-bordeaux1.fr, Charles-Henri.Bruneau@math.u-bordeaux1.fr

‡E-mail: marpeau@math.u-bordeaux1.fr, Fabien.Marpeau@math.u-bordeaux1.fr

§E-mail: saad@math.u-bordeaux1.fr, Mazen.Saad@math.u-bordeaux1.fr

Contract/grant sponsor: GdR MoMaS (CNRS), France

Received 9 November 2004

Revised 16 February 2005

Accepted 23 April 2005

tainers (for a mathematical point of view, see for e.g. Reference [1]). However, a leak is still possible.

In this work it is assumed that some radionuclides have escaped from their storage site and have started to contaminate the ground. At the usual depth the nuclear wastes are stocked, the ground is a water-saturated porous medium where the contaminants can be carried on by the flow. The main question is to know whether the radioactive pollution can reach the surface and consequently affect a population.

According to the slowness of porous media flows, experiments may be difficult or impossible. So, the numerical simulation is probably the best way to answer the question (see for e.g. References [2, 3]). It is now possible to simulate the dispersion of contaminants in large domains for millions of years. The difficulty is to use an approximation accurate enough to capture correctly the phenomena for such space and time scales.

The aim of this paper is to propose efficient schemes and algorithms to solve realistic benchmarks, in particular the COUPLEX 1 (see Reference [2] or the web page [4]) in a heterogeneous porous medium. The main result is the construction of a nearly second-order accurate scheme for the approximation of a convection–diffusion–reaction equation with a nonlinear term in the time derivative.

Next section is devoted to the modellization using Darcy's law for the flow and a system of convection–diffusion–reaction equations for the displacement of the radionuclides. The adsorption of the radio elements on the porous matrix is also taken into account and often leads to a nonlinear term in the time derivative. This last point is one of the major difficulties we have to deal with.

In Section 3, we present the whole approximation in two space dimensions with emphasis to the convection scheme which is studied in details. In addition to the nearly second-order accuracy, the scheme is proven to be positive and stable even if the medium is heterogeneous.

Beyond these mathematical results, numerical illustrations show at Section 4 that the approximation is relevant. Indeed it is observed that the schemes are robust enough to represent correctly the evolution of a contaminant through a discontinuity of the medium.

Finally, the end of the paper is devoted to COUPLEX 1 benchmark concerning a leak of a nuclear waste repository in a heterogeneous medium constituted of marl, limestone, clay and dogger rocks. Good results are obtained despite the strong discontinuities between these various layers.

2. THE MODEL

We consider a water saturated heterogeneous porous medium the porosity of which is denoted by ϕ .

According to de Marsily [5] and Bear [6], the miscible displacement of a free substratum s whose concentration in the water is c may be governed by the following convection–diffusion equation representing mass conservation:

$$\phi(X)\partial_t c(t, X) + \operatorname{div}(c(t, X)V(X)) - \operatorname{div}(D\nabla c(t, X)) = 0 \quad (1)$$

where t and $X \in \mathbb{R}^d$ denote, respectively, the time and space variables and $V = (V_i)_{i=1, \dots, d}$ is the filtration velocity. In this equation, $\operatorname{div}(c(t, X)V)$ represents the convection phenomenon while $\operatorname{div}(D\nabla c(t, X))$ stands for the diffusion–dispersion one. The tensor $D = d_m I + d_s$ is the sum of the effective diffusion taking into account both the molecular diffusion and the tortuosity

$d_m I$ with a positive coefficient and of the mechanical dispersion d_s [7–11]. The mechanical dispersion tensor is defined as

$$d_s = |V|(\alpha_l E(V) + \alpha_t(I - E(V))), \quad (E(V))_{ij} = \frac{V_i V_j}{|V|^2}$$

where the nonnegative constants α_l and α_t denote, respectively, the longitudinal and the transversal dispersion coefficients. Thus the diffusion–dispersion tensor D is finally coercive. Other forms can be found in Reference [10] or [12].

The heterogeneity of the medium implies that the coefficients ϕ , d_m , α_l and α_t depend on X but they are assumed to be constant in time.

The adsorption phenomenon can also be taken into account. We denote by F the adsorbed phase of the substratum s , and because it only occurs at the solid matrix, its contribution to the initial equation (1) leads to

$$\phi \partial_t c + (1 - \phi) \rho_s \partial_t F + \operatorname{div}(cV) - \operatorname{div}(D \nabla c) = 0 \quad (2)$$

where $\rho_s(X)$ is the density of the solid phase at location X . As the adsorption phenomenon is assumed to be instantaneous, F is a mapping of the nonnegative variable c and is called ‘adsorption isotherm’. In Reference [5] the author gives several examples of such isotherm F which are assumed to be functions of X to represent the heterogeneity of the medium:

$$\text{Linear isotherm} \quad : \quad F(X, c) = \gamma_1(X)c$$

$$\text{Quadratic isotherm} \quad : \quad F(X, c) = \gamma_1(X)c - \gamma_2(X)c^2$$

$$\text{Langmuir's isotherm} \quad : \quad F(X, c) = \frac{\gamma_1(X)c}{1 + \gamma_2(X)c}$$

$$\text{Freundlich's isotherm} \quad : \quad F(X, c) = \gamma_1(X)c^{1/n}$$

$$\text{Exponential isotherm} \quad : \quad c = \gamma_1(X)e^{\gamma_2(X)F(X,c)}$$

where $n \in \mathbb{N}^*$, γ_1 and γ_2 are nonnegative functions.

If the chemical species s is assumed to be radioactive, then it must lose its mass along the time. The radioactive decay factor of s is denoted by λ . As this phenomenon exists in both the aqueous and the adsorbed phases, the mass conservation equation finally writes

$$\phi(\partial_t c + \lambda c) + (1 - \phi)\rho_s(\partial_t F(X, c) + \lambda F(X, c)) + \operatorname{div}(cV) - \operatorname{div}(D \nabla c) = 0$$

But the disintegration of s may produce other chemical species of lower mass, and these other chemical species might also be radioactive and produce again and again other ones until the produced atom nucleus are stable. Thus a contamination by a finite number m of radionuclides s^k the concentrations of which are c^k has to be considered and yields to the following convection–diffusion–reaction system:

$$\begin{aligned} & \partial_t(\phi c^k + (1 - \phi)\rho_s F^k(X, c^k)) + \operatorname{div}(c^k V) - \operatorname{div}(D^k \nabla c^k) \\ & + \lambda^k(\phi c^k + (1 - \phi)\rho_s F^k(X, c^k)) - \sum_{\substack{l=1 \\ l \neq k}}^m \lambda^l \frac{M^k}{M_l} r_{kl}(\phi c^l + (1 - \phi)\rho_s F^l(X, c^l)) = 0 \end{aligned}$$

where M^k is the molar mass of s^k , r_{kl} denotes the production rate of s^k by s^l , and $\lambda^l = 0$ if s^l is not radioactive. Note that the adsorption isotherms and the diffusion–dispersion operators now depend on k . Since a nuclear reaction is irreversible, the m radionuclides can be ordered such that $R_{kl} = M^k/M_l r_{kl}$ is a lower triangular matrix with zero value on the main diagonal. Moreover, the sum of the coefficients of each row never overtakes 1.

As the contaminant does not change much the characteristics of the fluid, we assume that both the density ρ and the viscosity μ of the fluid are independent of the concentration vector and the filtration velocity V is given by Darcy’s law

$$V(t, X) = - \frac{K(X)}{\mu} (\nabla p(t, X) - \rho \mathbf{g}) \tag{3}$$

where p is the pressure, \mathbf{g} is the gravity vector, and $K \in \mathcal{M}_d(\mathbb{R})$ is the X -dependent permeability tensor. The Darcy law is valid in our case as we consider a porous medium of porosity smaller than 0.8 with small filtration velocities. Thus neither Brinkman equation nor Forchheimer terms are required [13]. Water being supposed incompressible, the free-divergence equation $\text{div}(V) = 0$ is imposed. In summary we have to solve the following set of equations for the pressure p , the velocity V and the concentrations vector $c = (c^1, \dots, c^m)^T$ as unknowns in an open bounded set $(0, T) \times \Omega$

$$\text{div} \left(-\frac{1}{\mu} K(X) (\nabla p(t, X) - \rho \mathbf{g}) \right) = 0 \tag{4}$$

$$V(t, X) = - \frac{1}{\mu} K(X) (\nabla p(t, X) - \rho \mathbf{g}) \tag{5}$$

$$\begin{aligned} \partial_t G^k(X, c^k(t, X)) + V(t, X) \nabla c^k(t, X) - \text{div}(D^k(X, V(t, X)) \nabla c^k(t, X)) \\ + \lambda^k G^k(X, c^k(t, X)) - \sum_{l=1}^k \lambda^l R_{kl} G^l(X, c^l(t, X)) = f^k(t, X), \quad \forall k = 1, \dots, m \end{aligned} \tag{6}$$

where the G^k are given by

$$G^k(X, c^k(t, X)) = \phi(X) c^k(t, X) + (1 - \phi(X)) \rho_s(X) F^k(X, c^k(t, X))$$

and the source terms $f^k(t, X)$ represent an eventual leak from a nuclear waste repository. To solve this system we need to add initial and boundary conditions that will be given for each numerical test.

3. APPROXIMATION

3.1. Generalities

In this section a method is described to approximate the system above in a two-dimensional space domain where the space variable is denoted by $X = (x, y)$. In all this work Ω is a rectangular domain $(0, L) \times (0, l)$. An accurate finite volume method is used on a uniform Cartesian grid with rectangular cells of size $\Delta x \times \Delta y$. The interval $(0, T)$ is split

into subintervals (t_n, t_{n+1}) and the time step Δt_n is defined by $t_{n+1} - t_n$ and will be denoted by Δt in all the sequel. Furthermore, we write $v_x = \Delta t / \Delta x$, $v_y = \Delta t / \Delta y$, and we set $x_i = (i - \frac{1}{2})\Delta x$, $y_j = (j - \frac{1}{2})\Delta y$, $x_{i+\frac{1}{2}} = i\Delta x$, $y_{j+\frac{1}{2}} = j\Delta y$ and

$$X_{i,j} = \begin{pmatrix} x_i \\ y_j \end{pmatrix}, \quad X_{i+\frac{1}{2},j} = \begin{pmatrix} x_{i+\frac{1}{2}} \\ y_j \end{pmatrix}, \quad X_{i,j+\frac{1}{2}} = \begin{pmatrix} x_i \\ y_{j+\frac{1}{2}} \end{pmatrix}, \quad X_{i+\frac{1}{2},j+\frac{1}{2}} = \begin{pmatrix} x_{i+\frac{1}{2}} \\ y_{j+\frac{1}{2}} \end{pmatrix}$$

The cells are assumed to be centred in $X_{i,j}$. A generic cell is denoted by $Q_{i,j} = (x_{i-\frac{1}{2}}, x_{i+\frac{1}{2}}) \times (y_{j-\frac{1}{2}}, y_{j+\frac{1}{2}})$ and $\Gamma_{i,j} = \partial Q_{i,j}$ (Figure 1). For every function ζ defined on $(0, T) \times \Omega$, $\zeta_{i,j}^n$, $\zeta_{i+\frac{1}{2},j}^n$, $\zeta_{i,j+\frac{1}{2}}^n$ and $\zeta_{i+\frac{1}{2},j+\frac{1}{2}}^n$ are, respectively, the approximations of $\zeta(t_n, X_{i,j})$, $\zeta(t_n, X_{i+\frac{1}{2},j})$, $\zeta(t_n, X_{i,j+\frac{1}{2}})$ and $\zeta(t_n, X_{i+\frac{1}{2},j+\frac{1}{2}})$ and the sequence $(\zeta_{i,j}^n)_{i,j}$ is denoted by ζ^n .

The approximate pressure $(p^n)_n$ and velocity $(V^n)_n$ are computed by solving, respectively, Equations (4) and (5) (see Section 3.2 for more details). Then starting from c^0 the approximate concentration vector c^{n+1} is obtained by the resolution of Equations (6) on the interval (t_n, t_{n+1}) with the given velocity V^n .

For the resolution of the convection–diffusion–reaction equations (6), two main difficulties arise. On the one hand, the presence of various differential operators makes our way towards the operator splitting technique so as to treat separately the convection and the diffusion–reaction terms as

$$\partial_t G^k(X, c^k) + V \nabla c^k = 0 \tag{7}$$

$$\partial_t G^k(X, c^k) - \text{div}(D^k \nabla c^k) + \lambda^k G^k(X, c^k) - \sum_{l=1}^k \lambda^l R_{kl} G^l(X, c^l) = f^k \tag{8}$$

If $c^{k,n}$ is the approximation of $c^k(t_n, \cdot)$, a first way to construct a splitting scheme for (7) and (8) would be to use the recurrent sequence

$$c^{k,n+1} = \mathcal{S}_2(\Delta t, \mathcal{S}_1(\Delta t, c^{k,n})) \tag{9}$$

where \mathcal{S}_1 and \mathcal{S}_2 are, respectively, approximation schemes for (7) and (8).

In the linear case it is proven in Reference [14] that such a way of splitting leads to a too large numerical error so that for every schemes \mathcal{S}_1 and \mathcal{S}_2 , the resulting scheme $\mathcal{S}_2 \circ \mathcal{S}_1$ becomes automatically a first-order accurate scheme in time. So the Strang splitting method of References [14, 15] is more appropriate. It is defined by

$$c^{k,n+1} = \mathcal{S}_1 \left(\frac{\Delta t}{2}, \mathcal{S}_2 \left(\Delta t, \mathcal{S}_1 \left(\frac{\Delta t}{2}, c^{k,n} \right) \right) \right) \tag{10}$$

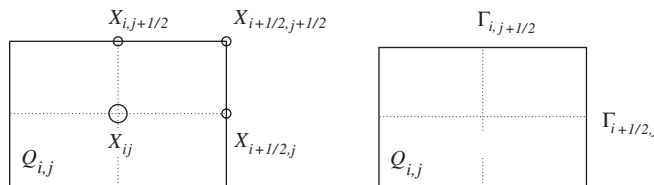


Figure 1. The cell $Q_{i,j}$.

and then in the linear case the additional error from this splitting technique to each scheme is only $\mathcal{O}(\Delta t^2)$. We use it by extension even if G^k is nonlinear.

On the other hand, we have to deal with the strong spatial heterogeneities of the porous medium modelling the ground. This will be discussed in Section 5 where a realistic test case is performed.

The main result of this work is presented in Section 3.3.2 where we adapt the numerical study of the hyperbolic systems of conservation laws summed up in Reference [16] to the nonlinear G^k case. Starting from a two-dimensional limitation technique [10, 17] for transport equations such that $\text{div } V = 0$, we build a nearly second-order accurate scheme approximating (7).

3.2. Approximation of the pressure and the filtration velocity

Darcy equation (4) at time t_n is solved in a classical way by a second-order finite volumes scheme on the cell $Q_{i,j}$. Hence the Stokes formula leads to

$$\begin{aligned} & - \int_{\Gamma_{i+\frac{1}{2},j}} \mathcal{K}(X) \partial_x p(t_n, X) \, dy + \int_{\Gamma_{i-\frac{1}{2},j}} \mathcal{K}(X) \partial_x p(t_n, X) \, dy \\ & - \int_{\Gamma_{i,j+\frac{1}{2}}} \mathcal{K}(X) (\partial_y p(t_n, X) + \rho g) \, dx + \int_{\Gamma_{i,j-\frac{1}{2}}} \mathcal{K}(X) (\partial_y p(t_n, X) + \rho g) \, dx = 0 \end{aligned}$$

where $\mathcal{K}(X) = (1/\mu)K(X)$. Then, the values of \mathcal{K} on the interfaces are evaluated with an harmonic average

$$\frac{1}{\mathcal{K}_{i+\frac{1}{2},j}} = \frac{1}{2} \left(\frac{1}{\mathcal{K}_{i,j}} + \frac{1}{\mathcal{K}_{i+1,j}} \right) \quad \text{and} \quad \frac{1}{\mathcal{K}_{i,j+\frac{1}{2}}} = \frac{1}{2} \left(\frac{1}{\mathcal{K}_{i,j}} + \frac{1}{\mathcal{K}_{i,j+1}} \right)$$

Then the space derivatives of the pressure are approximated by the centred second-order differences scheme, so that the corresponding scheme to compute the pressure reads as follows:

$$\begin{aligned} & \frac{\Delta y}{\Delta x} (\mathcal{K}_{i+\frac{1}{2},j} (p_{i,j}^n - p_{i+1,j}^n) + \mathcal{K}_{i-\frac{1}{2},j} (p_{i,j}^n - p_{i-1,j}^n)) + \frac{\Delta x}{\Delta y} (\mathcal{K}_{i,j+\frac{1}{2}} (p_{i,j}^n - p_{i,j+1}^n) \\ & + \mathcal{K}_{i,j-\frac{1}{2}} (p_{i,j}^n - p_{i,j-1}^n)) + \Delta x \rho g (\mathcal{K}_{i,j-\frac{1}{2}} - \mathcal{K}_{i,j+\frac{1}{2}}) = 0 \end{aligned} \tag{11}$$

The whole approximation yields a linear system $A p^n = L^n$, where L^n contains the Dirichlet or Neumann boundary conditions. The matrix A is a strongly dominant five diagonals matrix. The inversion of this system is carried out by the conjugated bi-gradient method, which needs to be preconditioned for a realistic heterogeneous porous medium (see Section 5).

The velocity $V = (u, v)$ is finally computed on the interfaces thanks to Equation (3) with the second-order centred scheme

$$u_{i+\frac{1}{2},j}^n = - \mathcal{K}_{i+\frac{1}{2},j} \frac{p_{i+1,j}^n - p_{i,j}^n}{\Delta x}; \quad v_{i,j+\frac{1}{2}}^n = - \mathcal{K}_{i,j+\frac{1}{2}} \left(\frac{p_{i,j+1}^n - p_{i,j}^n}{\Delta y} + \rho g \right)$$

Note that

$$\frac{1}{\Delta x}(u_{i+\frac{1}{2},j}^n - u_{i-\frac{1}{2},j}^n) + \frac{1}{\Delta y}(v_{i,j+\frac{1}{2}}^n - v_{i,j-\frac{1}{2}}^n) = 0$$

3.3. Approximation of the convection equation (7)

Let be

$$G: \begin{array}{ll} \Omega \times \mathbb{R} & \longrightarrow \mathbb{R} \\ (X, C) & \longmapsto G(X, C) \end{array}$$

a function such that

- $\forall X \in \Omega, G(X, 0) = 0,$
- $\forall X \in \Omega, C \mapsto G(X, C)$ is a continuous increasing bijective mapping.

We want to approximate the equation

$$\partial_t G(X, C(t, X)) + V(X) \cdot \nabla C(t, X) = 0 \quad (12)$$

For a porous medium modellization, such a mapping G represents

$$G(X, C) = \phi(X)C + (1 - \phi(X))\rho_s(X)F(X, C) \quad (13)$$

where C is a concentration and F is an usual adsorption isotherm. In the sequel $G^{-1}(X, C)$ denotes the unique real number such that $G(X, G^{-1}(X, C)) = C$.

Assuming C is constant on every cell Q_{ij} , we build a scheme of the form

$$G(X_{i,j}, C_{i,j}^{n+1}) = G(X_{i,j}, C_{i,j}^n) - \Delta t \mathcal{L}(X, C^n)$$

where \mathcal{L} is a mapping. Since G is bijective on \mathbb{R} , such a scheme is always well defined. Then, $C_{i,j}^{n+1}$ is obtained by inverting $G(X_{i,j}, C_{i,j}^{n+1})$. It remains to require these numerical solutions verify some physical properties such as positivity and boundedness. Note that without positivity the isotherm functions lose their meaning.

3.3.1. Classical first-order accurate schemes. The Upwind-like scheme: For any real z , we set

$$z^+ = \frac{|z| + z}{2} \quad \text{and} \quad z^- = \frac{|z| - z}{2}$$

so that $z^+ \geq 0$, $z^- \geq 0$ and $z = z^+ - z^-$. The classical upwind scheme can easily be extended to the nonlinear case. Equation (12) is discretized as follows:

$$G(X_{i,j}, C_{i,j}^{n+1}) = G(X_{i,j}, C_{i,j}^n) - v_x u_{i,j}^+ \Delta C_{i-\frac{1}{2},j}^n + v_x u_{i,j}^- \Delta C_{i+\frac{1}{2},j}^n - v_y v_{i,j}^+ \Delta C_{i,j-\frac{1}{2}}^n + v_y v_{i,j}^- \Delta C_{i,j+\frac{1}{2}}^n$$

where $\Delta C_{i+\frac{1}{2},j}^n = C_{i+1,j}^n - C_{i,j}^n$, $\Delta C_{i,j+\frac{1}{2}}^n = C_{i,j+1}^n - C_{i,j}^n$. According to Proposition 3 in Appendix A, the scheme is l^∞ -stable and positive under the CFL condition

$$\max_{i,j} \left(\frac{v_x |u_{i,j}| + v_y |v_{i,j}|}{\theta_{i,j}(G)} \right) \leq 1$$

where

$$\theta_{i,j}(G) = \min \left(\inf_{\substack{z_1, z_2 \in \mathbb{R}_+ \\ z_1 \neq z_2}} \left(\frac{G(X_{i,j}, z_1) - G(X_{i,j}, z_2)}{z_1 - z_2} \right), \inf_{\substack{z_1, z_2 \in \mathbb{R}_- \\ z_1 \neq z_2}} \left(\frac{G(X_{i,j}, z_1) - G(X_{i,j}, z_2)}{z_1 - z_2} \right) \right) \quad (14)$$

The linearized-transport-projection scheme: This first-order scheme built in this work is based on the Murman finite volume technique (see Appendix B). Assuming that $C \mapsto G(X, C)$ is differentiable, the quantity $1/\partial_C G(X, C)$ is denoted by $H(X, C)$, and sometimes, when it is not ambiguous, by $H(C)$. Then the scheme reads

$$\begin{aligned} G(X_{i,j}, C_{i,j}^{n+1}) &= G_{i,j}^{1,n} = G(X_{i,j}, C_{i,j}^n) \\ &- v_x \left(1 - \frac{v_y}{2} (v_{i,j+\frac{1}{2}}^+ H_{i,j+\frac{1}{2}}^n + v_{i,j-\frac{1}{2}}^- H_{i,j-\frac{1}{2}}^n) \right) (u_{i-\frac{1}{2},j}^+ \Delta C_{i-\frac{1}{2},j}^n - u_{i+\frac{1}{2},j}^- \Delta C_{i+\frac{1}{2},j}^n) \\ &- v_y \left(1 - \frac{v_x}{2} (u_{i+\frac{1}{2},j}^+ H_{i+\frac{1}{2},j}^n + u_{i-\frac{1}{2},j}^- H_{i-\frac{1}{2},j}^n) \right) (v_{i,j-\frac{1}{2}}^+ \Delta C_{i,j-\frac{1}{2}}^n - v_{i,j+\frac{1}{2}}^- \Delta C_{i,j+\frac{1}{2}}^n) \\ &- \frac{v_x v_y}{2} (u_{i+\frac{1}{2},j}^- H_{i+\frac{1}{2},j}^n (v_{i+1,j-\frac{1}{2}}^+ \Delta C_{i+1,j-\frac{1}{2}}^n - v_{i+1,j+\frac{1}{2}}^- \Delta C_{i+1,j+\frac{1}{2}}^n) \\ &+ u_{i-\frac{1}{2},j}^+ H_{i-\frac{1}{2},j}^n (v_{i-1,j-\frac{1}{2}}^+ \Delta C_{i-1,j-\frac{1}{2}}^n - v_{i-1,j+\frac{1}{2}}^- \Delta C_{i-1,j+\frac{1}{2}}^n) \\ &+ v_{i,j-\frac{1}{2}}^+ H_{i,j-\frac{1}{2}}^n (u_{i-\frac{1}{2},j-1}^+ \Delta C_{i-\frac{1}{2},j-1}^n - u_{i+\frac{1}{2},j-1}^- \Delta C_{i+\frac{1}{2},j-1}^n) \\ &+ v_{i,j+\frac{1}{2}}^- H_{i,j+\frac{1}{2}}^n (u_{i-\frac{1}{2},j+1}^+ \Delta C_{i-\frac{1}{2},j+1}^n - u_{i+\frac{1}{2},j+1}^- \Delta C_{i+\frac{1}{2},j+1}^n)) \end{aligned} \quad (15)$$

Proposition 1

Under the CFL conditions

$$\begin{aligned} \frac{v_y}{2} (v_{i,j+\frac{1}{2}}^+ H_{i,j+\frac{1}{2}} + v_{i,j-\frac{1}{2}}^- H_{i,j-\frac{1}{2}} + H_{i,\pm\frac{1}{2},j} (v_{i\pm 1,j+\frac{1}{2}}^- + v_{i\pm 1,j-\frac{1}{2}}^+)) &\leq 1 \\ \frac{v_x}{2} (u_{i+\frac{1}{2},j}^+ H_{i+\frac{1}{2},j} + u_{i-\frac{1}{2},j}^- H_{i-\frac{1}{2},j} + H_{i,j,\pm\frac{1}{2}} (u_{i+\frac{1}{2},j\pm 1}^- + u_{i-\frac{1}{2},j\pm 1}^+)) &\leq 1 \\ v_x (u_{i+\frac{1}{2},j}^- + u_{i-\frac{1}{2},j}^+) \left(1 - \frac{v_y}{2} (v_{i,j+\frac{1}{2}}^+ H_{i,j+\frac{1}{2}} + v_{i,j-\frac{1}{2}}^- H_{i,j-\frac{1}{2}}) \right) \\ + v_y (v_{i,j+\frac{1}{2}}^- + v_{i,j-\frac{1}{2}}^+) \left(1 - \frac{v_x}{2} (u_{i+\frac{1}{2},j}^+ H_{i+\frac{1}{2},j} + u_{i-\frac{1}{2},j}^- H_{i-\frac{1}{2},j}) \right) &\leq \theta_{i,j}(G) \end{aligned}$$

the linearized-transport-projection scheme (15) is both l^∞ -stable and positive.

This result comes directly from Proposition 3.

3.3.2. *A nearly second-order accurate limited scheme.* Our main result is presented here. Using the Lax–Wendroff technique, the aim of this paragraph is to adapt the method of References [10, 17] for a nonlinear G to construct a second-order accurate scheme. Starting from Taylor formula for G where time derivatives are replaced by space derivatives thanks to Equation (B1) in Appendix B we get

$$G(X, C(t_{n+1}, X)) = G(X, C(t_n, X)) - \Delta t V \cdot \nabla C + \frac{\Delta t^2}{2} \operatorname{div}(H(X, C) \operatorname{div}(CV)V) + \mathcal{O}(\Delta t^3)$$

Integrating the result on the cell $Q_{i,j}$ yields

$$\begin{aligned} \int_{Q_{ij}} G(X, C(t_{n+1}, X)) &= \int_{Q_{ij}} G(X, C(t_n, X)) - \Delta t \int_{Q_{ij}} V \cdot \nabla C \\ &+ \frac{\Delta t^2}{2} \int_{\Gamma_{ij}} H(X, C) \begin{pmatrix} u^2 & uv \\ uv & v^2 \end{pmatrix} \nabla C \cdot \mathbf{n} \, d\sigma + \int_{Q_{i,j}} \mathcal{O}(\Delta t^3) \end{aligned}$$

Finally, the spatial derivatives are approximated as in Reference [10] by centred finite differences schemes, taking into account the direction of the flow (remember H is always positive):

$$\begin{aligned} \int_{Q_{ij}} u \partial_x C \, dx \, dy &\approx \frac{\Delta y}{2} (u_{i+\frac{1}{2},j} \Delta C_{i+\frac{1}{2},j} + u_{i-\frac{1}{2},j} \Delta C_{i-\frac{1}{2},j}) \\ \int_{Q_{ij}} v \partial_y C \, dx \, dy &\approx \frac{\Delta x}{2} (v_{i,j+\frac{1}{2}} \Delta C_{i,j+\frac{1}{2}} + v_{i,j-\frac{1}{2}} \Delta C_{i,j-\frac{1}{2}}) \\ \int_{\Gamma_{i+\frac{1}{2},j}} H(C) u^2 \partial_x C \, dy &\approx \frac{\Delta y}{\Delta x} H_{i+\frac{1}{2},j} u_{i+\frac{1}{2},j}^2 \Delta C_{i+\frac{1}{2},j} \\ \int_{\Gamma_{i+\frac{1}{2},j}} H(C) uv \partial_y C \, dy &\approx L_{i+\frac{1}{2},j}^n \\ \int_{\Gamma_{i,j+\frac{1}{2}}} H(C) v^2 \partial_y C \, dx &\approx \frac{\Delta x}{\Delta y} H_{i,j+\frac{1}{2}} v_{i,j+\frac{1}{2}}^2 \Delta C_{i,j+\frac{1}{2}} \\ \int_{\Gamma_{i,j+\frac{1}{2}}} H(C) uv \partial_x C \, dx &\approx L_{i,j+\frac{1}{2}}^n \end{aligned}$$

where

$$\begin{aligned} L_{i+\frac{1}{2},j}^n &= \Delta y H_{i+\frac{1}{2},j}^n \frac{u_{i+\frac{1}{2},j}}{2} \begin{cases} v_{i,j+\frac{1}{2}} \Delta C_{i,j+\frac{1}{2}} + v_{i,j-\frac{1}{2}} \Delta C_{i,j-\frac{1}{2}} & \text{if } u_{i+\frac{1}{2},j} \geq 0 \\ v_{i+1,j+\frac{1}{2}} \Delta C_{i+1,j+\frac{1}{2}} + v_{i+1,j-\frac{1}{2}} \Delta C_{i+1,j-\frac{1}{2}} & \text{if } u_{i+\frac{1}{2},j} < 0 \end{cases} \\ L_{i,j+\frac{1}{2}}^n &= \Delta x H_{i,j+\frac{1}{2}}^n \frac{v_{i,j+\frac{1}{2}}}{2} \begin{cases} u_{i+\frac{1}{2},j} \Delta C_{i+\frac{1}{2},j} + u_{i-\frac{1}{2},j} \Delta C_{i-\frac{1}{2},j} & \text{if } v_{i,j+\frac{1}{2}} \geq 0 \\ u_{i+\frac{1}{2},j+1} \Delta C_{i+\frac{1}{2},j+1} + u_{i-\frac{1}{2},j+1} \Delta C_{i-\frac{1}{2},j+1} & \text{if } v_{i,j+\frac{1}{2}} < 0 \end{cases} \end{aligned}$$

The same argument on the other edges of $Q_{i,j}$ leads to the second-order accurate Lax–Wendroff-like scheme

$$\begin{aligned}
 G(X_{i,j}, C_{i,j}^{n+1}) &= G(X_{i,j}, C_{i,j}^n) - \frac{v_x}{2}(u_{i+\frac{1}{2},j}\Delta C_{i+\frac{1}{2},j} + u_{i-\frac{1}{2},j}\Delta C_{i-\frac{1}{2},j}) \\
 &\quad - \frac{v_y}{2}(v_{i,j+\frac{1}{2}}\Delta C_{i,j+\frac{1}{2}} + u_{i-\frac{1}{2},j}\Delta C_{i,j-\frac{1}{2}}) \\
 &\quad + \frac{v_x^2}{2}(H_{i+\frac{1}{2},j}^n u_{i+\frac{1}{2},j}^2 \Delta C_{i+\frac{1}{2},j} - H_{i-\frac{1}{2},j}^n u_{i-\frac{1}{2},j}^2 \Delta C_{i-\frac{1}{2},j}) \\
 &\quad + \frac{v_y^2}{2}(H_{i,j+\frac{1}{2}}^n v_{i,j+\frac{1}{2}}^2 \Delta C_{i,j+\frac{1}{2}} - H_{i,j-\frac{1}{2}}^n v_{i,j-\frac{1}{2}}^2 \Delta C_{i,j-\frac{1}{2}}) \\
 &\quad + \frac{v_x v_y}{2}(L_{i+\frac{1}{2},j}^n - L_{i-\frac{1}{2},j}^n) + \frac{v_x v_y}{2}(L_{i,j+\frac{1}{2}}^n - L_{i,j-\frac{1}{2}}^n) \tag{16}
 \end{aligned}$$

We make this scheme l^∞ -stable and positive thanks to Proposition 3 with usual 2D flux-limitation arguments. We refer the reader to References [18, 19]. We construct a limited scheme which is second-order accurate assuming $\text{div } V = 0$ (see Appendix C for more details). Let φ be a positive function such that

$$\varphi(x) \begin{cases} = 0 & \text{if } x \leq 0 \\ \leq \min(M, Mx) & \text{if } x > 0 \end{cases} \tag{17}$$

where $M \leq 2$. Introducing the following notations:

$$\begin{aligned}
 r_{i-\frac{1}{2},j}^{n-} &= \frac{u_{i+\frac{1}{2},j}^- \Delta C_{i+\frac{1}{2},j}^n}{u_{i-\frac{1}{2},j}^- \Delta C_{i-\frac{1}{2},j}^n}, & r_{i+\frac{1}{2},j}^{n+} &= \frac{u_{i-\frac{1}{2},j}^+ \Delta C_{i-\frac{1}{2},j}^n}{u_{i+\frac{1}{2},j}^+ \Delta C_{i+\frac{1}{2},j}^n} \\
 r_{i,j-\frac{1}{2}}^{n-} &= \frac{v_{i,j+\frac{1}{2}}^- \Delta C_{i,j+\frac{1}{2}}^n}{v_{i,j-\frac{1}{2}}^- \Delta C_{i,j-\frac{1}{2}}^n}, & r_{i,j+\frac{1}{2}}^{n+} &= \frac{v_{i,j-\frac{1}{2}}^+ \Delta C_{i,j-\frac{1}{2}}^n}{v_{i,j+\frac{1}{2}}^+ \Delta C_{i,j+\frac{1}{2}}^n} \\
 \varphi_{i+\frac{1}{2},j}^n &= \begin{cases} \varphi(r_{i+\frac{1}{2},j}^{n-}) & \text{if } u_{i+\frac{1}{2},j} \leq 0 \\ \varphi(r_{i+\frac{1}{2},j}^{n+}) & \text{if } u_{i+\frac{1}{2},j} > 0 \end{cases}, & \varphi_{i,j+\frac{1}{2}}^n &= \begin{cases} \varphi(r_{i,j+\frac{1}{2}}^{n-}) & \text{if } v_{i,j+\frac{1}{2}} \leq 0 \\ \varphi(r_{i,j+\frac{1}{2}}^{n+}) & \text{if } v_{i,j+\frac{1}{2}} > 0 \end{cases}
 \end{aligned}$$

and

$$\begin{aligned}
 \alpha_{i,j} &= 1 - \frac{v_y}{2}(v_{i,j+\frac{1}{2}}^+ H_{i,j+\frac{1}{2}}^n + v_{i,j-\frac{1}{2}}^- H_{i,j-\frac{1}{2}}^n), & \beta_{i,j} &= 1 - \frac{v_x}{2}(u_{i+\frac{1}{2},j}^+ H_{i+\frac{1}{2},j}^n + u_{i-\frac{1}{2},j}^- H_{i-\frac{1}{2},j}^n) \tag{18} \\
 \tilde{\kappa}_{i+\frac{1}{2},j} &= \max(v_x |u_{i+\frac{1}{2},j}|, v_y (v_{i+1,j-\frac{1}{2}}^+ + v_{i+1,j+\frac{1}{2}}^-), v_y (v_{i-1,j-\frac{1}{2}}^+ + v_{i-1,j+\frac{1}{2}}^-)) \\
 \tilde{\kappa}_{i,j+\frac{1}{2}} &= \max(v_y |v_{i,j+\frac{1}{2}}|, v_x (u_{i+\frac{1}{2},j+1}^- + u_{i-\frac{1}{2},j+1}^+), v_x (u_{i-\frac{1}{2},j-1}^+ + u_{i+\frac{1}{2},j-1}^-))
 \end{aligned}$$

we get the following nearly second-order limited scheme that is written down as an extension of the previous first-order scheme:

$$\begin{aligned}
& G(X_{i,j}, C_{i,j}^{n+1}) \\
&= G_{i,j}^{1,n} - \frac{v_x}{2} (|u_{i+\frac{1}{2},j}|(\alpha_{i,j} - \tilde{\kappa}_{i+\frac{1}{2},j})\varphi_{i+\frac{1}{2},j}^n \Delta C_{i+\frac{1}{2},j}^n - |u_{i-\frac{1}{2},j}|(\alpha_{i,j} - \tilde{\kappa}_{i-\frac{1}{2},j})\varphi_{i-\frac{1}{2},j}^n \Delta C_{i-\frac{1}{2},j}^n) \\
&\quad - \frac{v_y}{2} (|v_{i,j+\frac{1}{2}}|(\beta_{i,j} - \tilde{\kappa}_{i,j+\frac{1}{2}})\varphi_{i,j+\frac{1}{2}}^n \Delta C_{i,j+\frac{1}{2}}^n - |v_{i,j-\frac{1}{2}}|(\beta_{i,j} - \tilde{\kappa}_{i,j-\frac{1}{2}})\varphi_{i,j-\frac{1}{2}}^n \Delta C_{i,j-\frac{1}{2}}^n) \\
&\quad + \frac{v_x v_y}{4} (H_{i+\frac{1}{2},j}^n u_{i+\frac{1}{2},j}^- (|v_{i+1,j-\frac{1}{2}}|\varphi_{i+1,j-\frac{1}{2}}^n \Delta C_{i+1,j-\frac{1}{2}}^n - |v_{i+1,j+\frac{1}{2}}|\varphi_{i+1,j+\frac{1}{2}}^n \Delta C_{i+1,j+\frac{1}{2}}^n) \\
&\quad + H_{i-\frac{1}{2},j}^n u_{i-\frac{1}{2},j}^+ (|v_{i-1,j-\frac{1}{2}}|\varphi_{i-1,j-\frac{1}{2}}^n \Delta C_{i-1,j-\frac{1}{2}}^n - |v_{i-1,j+\frac{1}{2}}|\varphi_{i-1,j+\frac{1}{2}}^n \Delta C_{i-1,j+\frac{1}{2}}^n) \\
&\quad + H_{i,j+\frac{1}{2}}^n v_{i,j+\frac{1}{2}}^- (|u_{i-\frac{1}{2},j+1}|\varphi_{i-\frac{1}{2},j+1}^n \Delta C_{i-\frac{1}{2},j+1}^n - |u_{i+\frac{1}{2},j+1}|\varphi_{i+\frac{1}{2},j+1}^n \Delta C_{i+\frac{1}{2},j+1}^n) \\
&\quad + H_{i,j-\frac{1}{2}}^n v_{i,j-\frac{1}{2}}^+ (|u_{i-\frac{1}{2},j-1}|\varphi_{i-\frac{1}{2},j-1}^n \Delta C_{i-\frac{1}{2},j-1}^n - |u_{i+\frac{1}{2},j-1}|\varphi_{i+\frac{1}{2},j-1}^n \Delta C_{i+\frac{1}{2},j-1}^n)) \quad (19)
\end{aligned}$$

Proposition 2

Under the following CFL conditions:

$$\begin{aligned}
& \Delta t \left(\frac{1}{2\Delta y} (v_{i,j+\frac{1}{2}}^+ H_{i,j+\frac{1}{2}}^n + v_{i,j-\frac{1}{2}}^- H_{i,j-\frac{1}{2}}^n) \right. \\
& \quad \left. + \max \left(\frac{1}{\Delta x} |u_{i\pm\frac{1}{2},j}| H_{i\pm\frac{1}{2},j}^n, \frac{1}{\Delta y} (v_{i+1,j-\frac{1}{2}}^+ + v_{i+1,j+\frac{1}{2}}^-), \frac{1}{\Delta y} (v_{i-1,j-\frac{1}{2}}^+ + v_{i-1,j+\frac{1}{2}}^-) \right) \right) \leq 1 \quad (20)
\end{aligned}$$

$$\begin{aligned}
& \Delta t \left(\frac{1}{2\Delta x} (u_{i+\frac{1}{2},j}^+ H_{i+\frac{1}{2},j}^n + u_{i-\frac{1}{2},j}^- H_{i-\frac{1}{2},j}^n) \right. \\
& \quad \left. + \max \left(\frac{1}{\Delta y} |v_{i,j\pm\frac{1}{2}}| H_{i,j\pm\frac{1}{2}}^n, \frac{1}{\Delta x} (u_{i+\frac{1}{2},j+1}^- + u_{i-\frac{1}{2},j+1}^+), \frac{1}{\Delta x} (u_{i-\frac{1}{2},j-1}^+ + u_{i+\frac{1}{2},j-1}^-) \right) \right) \leq 1 \quad (21)
\end{aligned}$$

$$\begin{aligned}
& \frac{1}{\theta_{i,j}(G)} (v_x u_{i+\frac{1}{2},j}^- (2\alpha_{i,j} - \tilde{\kappa}_{i-\frac{1}{2},j} H_{i-\frac{1}{2},j}^n) + v_x u_{i-\frac{1}{2},j}^+ (2\alpha_{i,j} - \tilde{\kappa}_{i+\frac{1}{2},j} H_{i+\frac{1}{2},j}^n) \\
& \quad + v_y v_{i,j+\frac{1}{2}}^- (2\beta_{i,j} - \tilde{\kappa}_{i,j-\frac{1}{2}} H_{i,j-\frac{1}{2}}^n) + v_y v_{i,j-\frac{1}{2}}^+ (2\beta_{i,j} - \tilde{\kappa}_{i,j+\frac{1}{2}} H_{i,j+\frac{1}{2}}^n)) \leq 1 \quad (22)
\end{aligned}$$

the nearly second-order scheme (19) is l^∞ -stable and positive.

The proof of this proposition is detailed in Appendix C. In the same way it is possible to improve the order of the scheme, for instance to third-order following Reference [17] but the present scheme is much easier to implement and gives satisfactory results on the classical test cases. Usual flux limiters are recalled

$$\text{Roe's limiters : } \varphi(r) = \max(0, \min(\Phi r, 1), \min(\Phi, r)) \quad \text{where } 1 \leq \Phi \leq 2$$

For $\Phi = 1$, such a φ is called the Minmod limiter. For $\Phi = 2$, it corresponds to the Superbee limiter

$$\text{Van Leer's limiter : } \varphi(r) = \begin{cases} 0 & \text{if } r \leq 0 \\ \frac{2r}{1+r} & \text{if } r \geq 0 \end{cases}$$

3.4. Approximation of the reaction–diffusion equation (8)

Let S be a radionuclide of concentration C generated by a finite number k of other elements that are called s^l , $l = 1, \dots, k$, the concentrations of which are denoted, respectively, by c^l . The following reaction–diffusion equation on the unknown C is considered

$$\partial_t G(X, C) - \operatorname{div}(D(X, V(X)) \nabla C) + \lambda G(X, C) - \sum_{l=1}^k \lambda^l R_l G^l(X, c^l) = f(t, X)$$

Note that if C denotes the concentration of a specie s^k in Equation (6), then the coefficient R_l stands for the real number R_{kl} , while f and λ are related to f^k and λ^k . Concentration C is assumed known at time t_n .

First, the time derivative term $\partial_t G(X, C)$ is approximated at first-order by Euler scheme

$$\partial_t G(X, C) \approx \frac{G(X, C^{n+1}) - G(X, C^n)}{\Delta t}$$

Next, to avoid a too restrictive CFL condition, the diffusion operator $\operatorname{div}(D \nabla C)$ is treated implicitly, as well as the other terms. Note in addition that since the matrix R is lower triangular with zero value on the main diagonal, Equations (6) can be solved sequentially from the first one, so that $\sum_{l=1}^k \lambda^l R_l G^l(X, c^l)$ is known at time t_{n+1} and thus can be treated implicitly without any difficulty. The equation

$$\begin{aligned} & \frac{G(X, C(t_{n+1}, X)) - G(X, C(t_n, X))}{\Delta t} - \operatorname{div}(D(X, V(X)) \nabla C(t_{n+1}, X)) \\ & + \lambda G(X, C(t_{n+1}, X)) - \sum_{l=1}^k \lambda^l R_l G^l(X, c^l(t_{n+1}, X)) = f(t_{n+1}, X) \end{aligned}$$

is integrated on the cell $Q_{i,j}$. The velocities components $u_{i \pm \frac{1}{2}, j}$ and $v_{i, j \pm \frac{1}{2}}$ are given and the scheme developed in Reference [10] yields using the Stokes formula as the tensor D

is symmetric

$$\begin{aligned} \int_{Q_{i,j}} \operatorname{div}(D\nabla C) &= \int_{\Gamma_{i+\frac{1}{2},j}} (D^{11}\partial_x C + D^{12}\partial_y C) dy - \int_{\Gamma_{i-\frac{1}{2},j}} (D^{11}\partial_x C + D^{12}\partial_y C) dy \\ &\quad + \int_{\Gamma_{i,j+\frac{1}{2}}} (D^{12}\partial_x C + D^{22}\partial_y C) dx - \int_{\Gamma_{i,j-\frac{1}{2}}} (D^{12}\partial_x C + D^{22}\partial_y C) dx \end{aligned}$$

where $\partial_x C = \partial_x C(t_{n+1}, X)$ and $\partial_y C = \partial_y C(t_{n+1}, X)$. The space derivatives are then approximated by the second-order accurate centred finite differences scheme as

$$\begin{aligned} \int_{\Gamma_{i+\frac{1}{2},j}} D^{11}\partial_x C dy &\approx \frac{\Delta y}{\Delta x} D_{i+\frac{1}{2},j}^{11} (C_{i+1,j}^{n+1} - C_{i,j}^{n+1}) \\ \int_{\Gamma_{i+\frac{1}{2},j}} D^{12}\partial_y C dy &\approx \frac{1}{2} D_{i+\frac{1}{2},j+\frac{1}{2}}^{12} (C_{i+\frac{1}{2},j+1}^{n+1} - C_{i+\frac{1}{2},j}^{n+1}) + \frac{1}{2} D_{i+\frac{1}{2},j-\frac{1}{2}}^{12} (C_{i+\frac{1}{2},j}^{n+1} - C_{i+\frac{1}{2},j-1}^{n+1}) \\ \int_{\Gamma_{i,j+\frac{1}{2}}} D^{12}\partial_x C dx &\approx \frac{1}{2} D_{i+\frac{1}{2},j+\frac{1}{2}}^{12} (C_{i+1,j+\frac{1}{2}}^{n+1} - C_{i,j+\frac{1}{2}}^{n+1}) + \frac{1}{2} D_{i-\frac{1}{2},j+\frac{1}{2}}^{12} (C_{i,j+\frac{1}{2}}^{n+1} - C_{i-1,j+\frac{1}{2}}^{n+1}) \\ \int_{\Gamma_{i,j+\frac{1}{2}}} D^{22}\partial_y C dx &\approx \frac{\Delta x}{\Delta y} D_{i,j+\frac{1}{2}}^{22} (C_{i,j+1}^{n+1} - C_{i,j}^{n+1}) \end{aligned}$$

where $D_{i+\frac{1}{2},j}^{11}$, $D_{i\pm\frac{1}{2},j\pm\frac{1}{2}}^{12}$ and $D_{i,j+\frac{1}{2}}^{22}$ are the coefficients of D evaluated using the velocities $u_{i+\frac{1}{2},j}$, $v_{i,j+\frac{1}{2}}$ and

$$\begin{aligned} u_{i,j+\frac{1}{2}} &= \frac{1}{4}(u_{i+\frac{1}{2},j} + u_{i-\frac{1}{2},j} + u_{i-\frac{1}{2},j+1} + u_{i+\frac{1}{2},j+1}) \\ v_{i+\frac{1}{2},j} &= \frac{1}{4}(v_{i,j+\frac{1}{2}} + v_{i,j-\frac{1}{2}} + v_{i+1,j+\frac{1}{2}} + v_{i+1,j-\frac{1}{2}}) \\ u_{i\pm\frac{1}{2},j\pm\frac{1}{2}} &= \frac{1}{2}(u_{i\pm\frac{1}{2},j} + u_{i\pm\frac{1}{2},j\pm 1}) \\ v_{i\pm\frac{1}{2},j\pm\frac{1}{2}} &= \frac{1}{2}(v_{i,j\pm\frac{1}{2}} + v_{i\pm 1,j\pm\frac{1}{2}}) \end{aligned}$$

This process is repeated on the other edges of $Q_{i,j}$ giving the scheme:

$$\begin{aligned} (1 + \lambda\Delta t)G(X_{i,j}, C_{i,j}^{n+1}) + \Delta t\mathcal{L}(C^{n+1}) \\ = G(X_{i,j}, C_{i,j}^n) + \Delta t \sum_{l=1}^k \lambda^l R_l G^l(X_{i,j}, c_{i,j}^{l,n+1}) + \Delta t f_{i,j}^{n+1} \end{aligned} \quad (23)$$

where

$$\begin{aligned} \mathcal{L}(C^{n+1}) &= -\frac{1}{\Delta x^2} (D_{i+\frac{1}{2},j}^{11} (C_{i+1,j}^{n+1} - C_{i,j}^{n+1}) - D_{i-\frac{1}{2},j}^{11} (C_{i,j}^{n+1} - C_{i-1,j}^{n+1})) \\ &\quad -\frac{1}{\Delta y^2} (D_{i,j+\frac{1}{2}}^{22} (C_{i,j+1}^{n+1} - C_{i,j}^{n+1}) - D_{i,j-\frac{1}{2}}^{22} (C_{i,j}^{n+1} - C_{i,j-1}^{n+1})) \end{aligned}$$

$$\begin{aligned}
& -\frac{1}{2\Delta x\Delta y}(D_{i+\frac{1}{2},j+\frac{1}{2}}^{12}(C_{i+1,j+1}^{n+1} - C_{i,j}^{n+1}) - D_{i-\frac{1}{2},j-\frac{1}{2}}^{12}(C_{i,j}^{n+1} - C_{i-1,j-1}^{n+1})) \\
& +\frac{1}{2\Delta x\Delta y}(D_{i+\frac{1}{2},j-\frac{1}{2}}^{12}(C_{i+1,j-1}^{n+1} - C_{i,j}^{n+1}) - D_{i-\frac{1}{2},j+\frac{1}{2}}^{12}(C_{i,j}^{n+1} - C_{i-1,j+1}^{n+1}))
\end{aligned}$$

This implicit scheme leads to a nonlinear system if G is nonlinear, or to a linear system otherwise. A Newton method is chosen to inverse this system. The Jacobian matrices are nine diagonals. Let us note that for realistic coefficients and realistic velocities of porous media flows, the effective diffusion often predominates the mechanical dispersion, so that the coefficients D^{11} and D^{22} are often upper than D^{12} . But this is not enough to prove the positivity of the scheme. When D^{12} is constant it is easy to get the positivity and stability of the scheme but since in general it is not, the space contributions do not lead to a diagonal dominant matrix. However, thanks to the time term the quantity $\phi/\Delta t$ can dominate the extra terms under a CFL condition. For a realistic heterogeneous porous medium flow the CFL condition given by the advection term can be used to solve the problem. The conjugate bi-gradient method converges and the Jacobian matrices are preconditioned to improve the performance.

4. NUMERICAL TESTS

This section is devoted to show the robustness of the schemes built in the previous section to solve the convection–diffusion–reaction equation, by means of classical tests cases involving a constant velocity field such that $\text{div } V = 0$. Here the geometry is very simple and the heterogeneities are quite weak, so that these tests do not represent a real porous medium. Nevertheless they allow to quantify the accuracy of the schemes. A more realistic test case is proposed in the next section.

4.1. Classical convection in a circular velocity field

First, we use the limited scheme of Section 3.3.2 to solve the classical convection equation

$$\partial_t C + V \cdot \nabla C = 0$$

coupled to the usual boundary conditions. Setting $\Omega = (0, 1) \times (0, 1)$, the velocity field is supposed circular and centred at $(\frac{1}{2}, \frac{1}{2})$

$$V = (-2\pi(y - \frac{1}{2}), 2\pi(x - \frac{1}{2}))$$

The initial condition for C is given by $C = 1$ in the disk $(x - 0.25)^2 + (y - 0.5)^2 \leq 0.0036$, and $C = 0$ elsewhere. The CFL number is taken equal to 1 and the mesh is defined by the 100×100 uniform Cartesian grid. The solution of some schemes are plotted at $t = 1$ for which the exact solution is the same than the initial condition (Figure 2). After these results we decide to use in the following the second-order Superbee-limited scheme which is the more accurate. Note that similar results are obtained with a linear adsorption G .

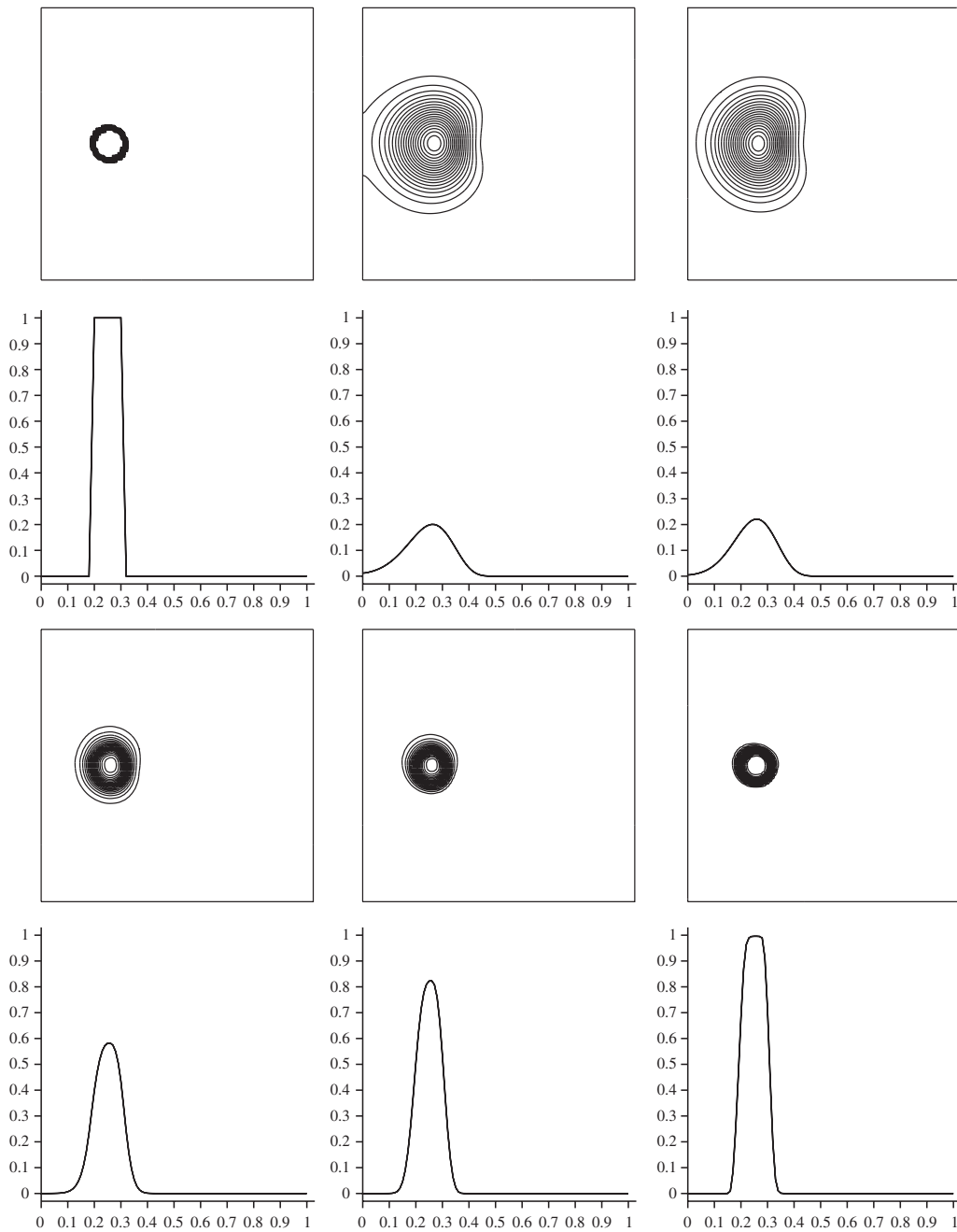


Figure 2. Concentration contours and cross section along the axis $y = \frac{1}{2}$ after one turn for the exact solution (top-left), the upwind-like scheme (top-center), the transport-projection scheme (15) (top-right), the present nearly second-order scheme with Minmod (bottom-left), Van Leer (bottom-center) and Superbee limiters (bottom-right). Twenty isovalues are plotted between the extrema.

4.2. Nonlinear convection in a homogeneous porous medium

We test now our scheme for a nonlinear adsorption G on the same domain and mesh. The porosity, the density of the solid matrix and the velocity are assumed to be constant: $\phi = 0.5$, $\rho_s = 1$ and $V = (1, 0.7)$.

The adsorption isotherm is defined by the quadratic law

$$F(X, C) = \frac{1}{2} C - \frac{1}{4} C^2$$

and we have to solve the following equation:

$$\partial_t(\phi C + (1 - \phi)\rho_s(\frac{1}{2} C - \frac{1}{4} C^2)) + V \cdot \nabla C = 0$$

The initial condition is given by $C = 1$ in the disk $(x - 0.2)^2 + (y - 0.2)^2 \leq 0.01$, and $C = 0$ elsewhere. The results are plotted on Figure 3. We observe clearly the retardation phenomenon due to the adsorption. The solution presents a shock in front of the contaminant and an expansion wave behind it. This is an obvious consequence of the concavity of the adsorption mapping. Let us note that the grid convergence is almost achieved as about the same results are obtained on a 200×100 mesh.

4.3. Classical convection in a heterogeneous porous medium

Finally the scheme is tested for a heterogeneous porous medium on the same domain and mesh. The porosity is assumed to be discontinuous across the line $y = -\frac{0.78}{0.79}x + 0.78$. The value of the porosity is denoted by ϕ_g under this line and by ϕ_d above. The equation

$$\phi \partial_t C + V \cdot \nabla C = 0 \quad \text{for } V = (0.3, 0.5)$$

is solved. The initial condition has the value 1 on the square $(0.1, 0.3) \times (0.1, 0.3)$ and 0 elsewhere (see Figure 4).

Two sets of porosity are chosen $\phi_g = 0.6$, $\phi_d = 0.3$ and $\phi_g = 0.3$, $\phi_d = 0.6$. The corresponding results are plotted in Figures 5 and 6. A discontinuity of the porosity coefficient ϕ is generally difficult to handle but the results obtained with our scheme are relevant. Indeed the contaminant crosses properly the discontinuity and a symmetric solution is recovered



Figure 3. Convection in an oblique velocity field with a quadratic adsorption. Concentration contours of the initial condition (left), numerical solution at times $t = 0.2$ (centre) and $t = 0.4$ (right), using twenty isovalues between 0 and 1.

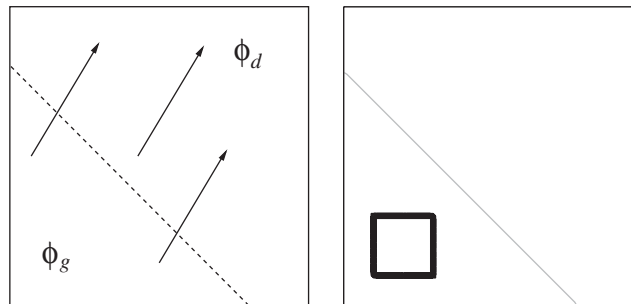


Figure 4. Geometry and initial condition for the discontinuous porosity convection problem.

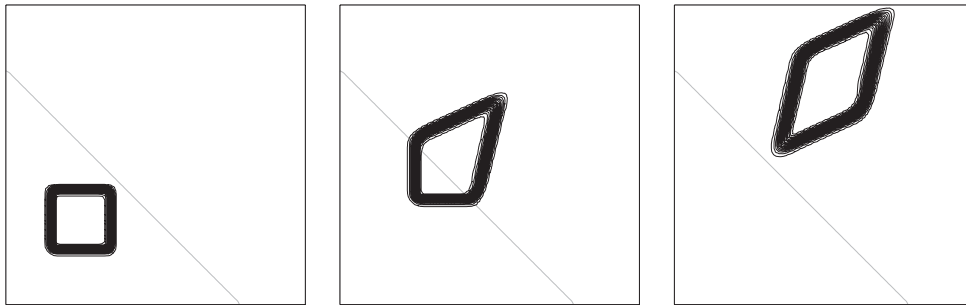


Figure 5. Numerical solution with $\phi_g = 0.6$ and $\phi_d = 0.3$ at times $t = 0.1$ (left), $t = 0.3$ (centre) and $t = 0.47$ (right), using twenty isovalues between 0 and 1.

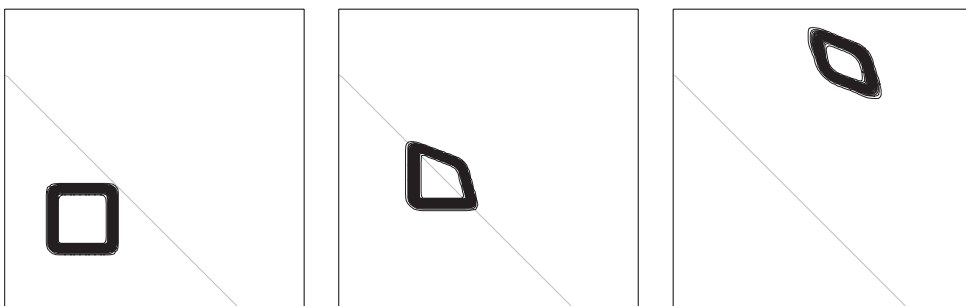


Figure 6. Numerical solution with $\phi_g = 0.3$ and $\phi_d = 0.6$ at times $t = 0.06$ (left), $t = 0.15$ (centre) and $t = 0.6$ (right), using twenty isovalues between 0 and 1.

beyond in both cases. This is quite normal because Proposition 2 does not require any homogeneity of the medium.

In the first case the contaminant spreads because the porosity becomes twice smaller and consequently the effective velocity of the contaminant becomes twice faster. On the contrary,

in the second case the curve is compressed. Nevertheless, in both cases the mass $\int_{\Omega} G(X, C) dX$ remains unchanged along the time.

4.4. Convection–diffusion–reaction in a heterogeneous porous medium with a nonlinear adsorption

The last test case of this section couples convection, diffusion and reaction phenomena in a heterogeneous porous medium (Equation (6)) on the same domain and mesh. The medium is discontinuous on both sides of the line $y=x$. The region above this line is denoted by Ω_1 , and the region underneath is denoted by Ω_2 . The porosity is 0.3 for Ω_1 , and 0.2 for Ω_2 . The velocity field is defined by

$$V = \left(-\frac{\pi}{50} \left(y - \frac{1}{2} \right), \frac{\pi}{50} \left(x - \frac{1}{2} \right) \right)$$

The displacement of two chemical species s^1 and s^2 is studied. The species s^1 is assumed radioactive, with 14 as molar mass. Its decay factor λ^1 is such that $\lambda^1 = \ln 2/T^1$, where the period $T^1 = 15$. The species s^2 is assumed stable ($\lambda^2 = 0$) with 12 as molar mass, and is generated by filiation from the element s^1 with the rate 90%. The diffusion–dispersion tensor

$$D^k = d_m^k I + |V|(\alpha_l^k E(V) + \alpha_t^k (I - E(V))), \quad (E(V))_{ij} = \frac{V_i V_j}{|V|^2}$$

is independent of k and its values are given in the Table I.

The adsorption isotherm for s^1 is linear in Ω_1 as $F^1(x, c^1) = \frac{1}{10} c^1$, and Langmuir-like in Ω_2 as $F^1(x, c^1) = \frac{1}{10} (c^1/1 + c^1)$. The species s^2 is assumed unadsorbated ($F^2(x, c^2) = 0$ in Ω). The boundary conditions are $D^k \nabla c^k \cdot \mathbf{n} - c^k V \cdot \mathbf{n} = 0$ everywhere on the boundary. The initial condition for s^1 is $c^1 = 1$ in the disk $(x - 0.2)^2 + (y - 0.5)^2 = 0.01$ and $c^1 = 0$ elsewhere. The value c^2 at $t = 0$ is zero everywhere (see Figure 7). Obviously the geological coefficients presented here are not realistic in comparison with a ground, but nevertheless they allow to observe that the scheme can take into account all the phenomena described in Section 2. Solutions at times 2, 5 and 14 are plotted in Figure 8. We can observe that although s^2 is not present at $t = 0$, it is produced by the destruction of s^1 . Thus by the way of the radioactivity s^1 loses its mass along the time whereas s^2 increases its one as Figure 9 shows. The different phenomena are well captured, in particular the species s^2 goes faster as there is no delay due to the adsorption as for the species s^1 . Moreover, the diffusion of the species is clearly observed.

Table I. Value of the diffusion and dispersion coefficients.

	d_m^k	α_l^k	α_t^k
Ω_1	0.00001	0.00005	0.00002
Ω_2	0.000001	0.00001	0.000005

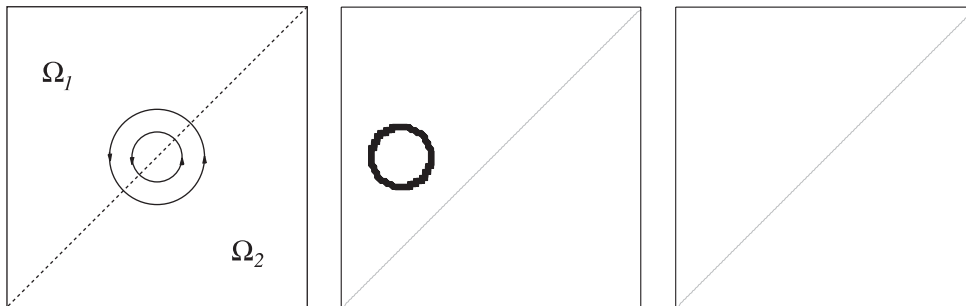


Figure 7. Geometry for the convection–diffusion–reaction test-case (left), initial conditions for s^1 (centre), and for s^2 (right).

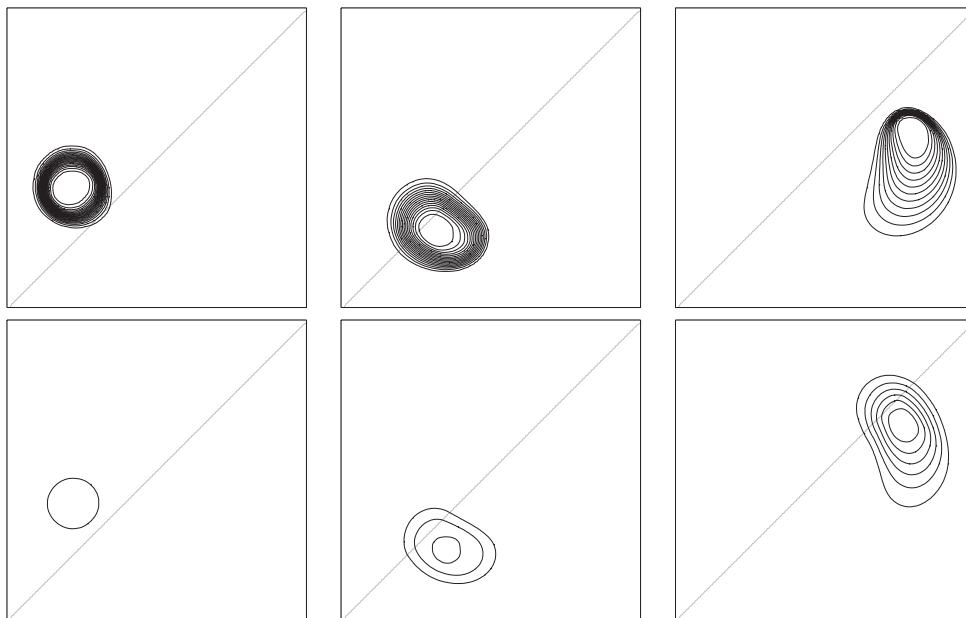


Figure 8. Concentration contours c^1 (top) and c^2 (bottom) for the convection–diffusion–reaction problem at times $t = 2$ (left), $t = 5$ (centre) and $t = 14$ (right). Twenty isovalues between 0 and 1 are plotted.

Remark

In this last test case a splitting is needed and we can then compare the two splittings given in Section 3. An iteration of the Strang splitting scheme (10) is more expensive than one of the classical splitting scheme (9) but the Strang splitting scheme can be implemented with a CFL number twice greater than the one of the classical splitting scheme. Finally, it converges faster in terms of CPU time.

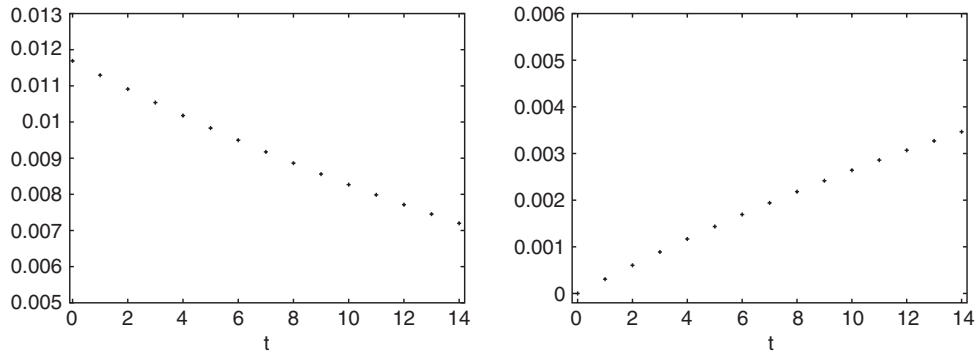


Figure 9. Mass of s^1 (left) and s^2 (right) along the time.

5. THE COUPLEX 1 TEST CASE

This section presents the final test of this work where the ground is represented by several geological layers. The additional difficulty in comparison to the previous computations is the presence of strong heterogeneities that exist in the ground porous matrix. For example, the permeability of clay rocks can be thousand or million times smaller than limestone ones, and so the finite volumes matrix of the scheme (11) can be very ill-conditioned. Moreover, the effective diffusion d_m , and the mechanical diffusion α_l and α_t of the tensor D can also be thousand times greater from one rock to another. Thus the Jacobian matrices of the scheme (23) are also often ill-conditioned. So it leads to precondition the matrices and we choose the incomplete factorization of Gauss.

This benchmark has been proposed in 2001 by the French ANDRA to study the safety of the nuclear waste repositories in the ground (see References [2, 4]). This test concerns the displacement in the underground of the Iodine ^{129}I and plutonium ^{242}Pu elements which come from a leak in a nuclear waste repository that lies into a clay layer. This clay layer is round off by a dogger and a limestone layer. The near ground is made of some marl rocks. The geometry of this test is drawn on Figure 10. The repository \mathcal{R} is modelled by the rectangular uniform injection well

$$\mathcal{R} = \{(x, y) \in [18440, 21680] \times [244, 250]\}$$

Note that the width of the domain is quite small in comparison with its length. Furthermore, the width of the repository (6 m) is also very small compared with the width of the domain (695 m), and this is a restriction for the uniform mesh we want to use, but such a mesh is suitable to keep the accuracy of the approximation. Finally, because of the slowness of the flow, the time scaling is chosen very long ($T = 10^7$ years) in comparison with the space scaling. But the radio-elements leak from the repository over a small period compared with T (see Figure 11).

As the boundary conditions for pressure and velocity fields are assumed independent of time, the flow is also independent of time. The permeability tensor is the diagonal matrix $K = K_e I$, where K_e is called the permeability coefficient. Setting $k_e = \rho g K_e / \mu$, the hydrodynamic load is defined by $h = \frac{p}{\rho g} + y$, so $V = -k_e \nabla h$ and $\text{div}(-k_e \nabla h) = 0$. This equation in the h variable

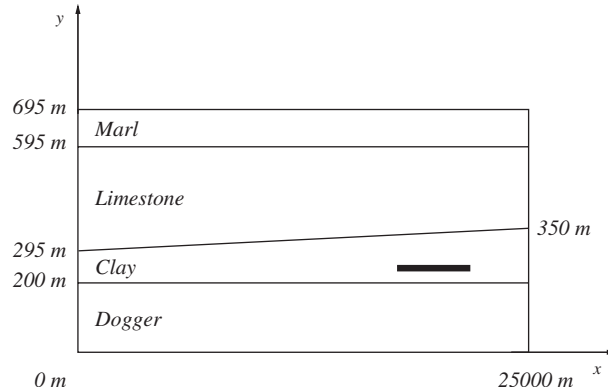
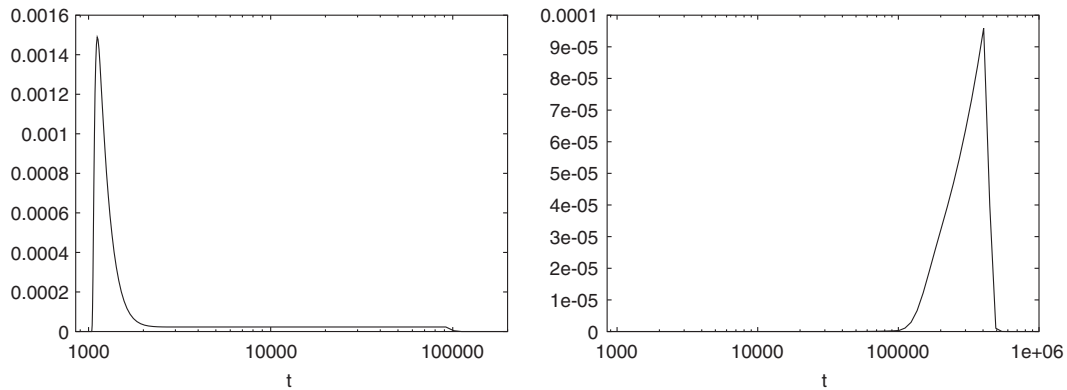


Figure 10. Geometry for the COUPLEX 1 test-case.

Figure 11. Source terms f^1 (left) and f^2 (right) along the time.

does not lead to an additional difficulty compared to Equation (4) as the following set of boundary conditions is specified:

$$\begin{aligned}
 h &= 289 && \text{on } \{25000\} \times [0, 200] \\
 h &= 310 && \text{on } \{25000\} \times [350, 595] \\
 h &= 180 + 160x/25000 && \text{on } [0, 25000] \times \{695\} \\
 h &= 200 && \text{on } \{0\} \times [295, 595] \\
 h &= 200 && \text{on } \{0\} \times [0, 200] \\
 V \cdot \mathbf{n} &= 0 && \text{elsewhere}
 \end{aligned}$$

The coefficient k_e is defined in Table II.

Table II. Value of the intrinsic permeabilities.

	Marl	Limestone	Clay	Dogger
k_e (m/year)	3.1536×10^{-5}	6.3072	3.1536×10^{-6}	25.2288

Table III. Value of the diffusion and dispersion coefficients.

	^{129}I			^{242}Pu		
	d_m^1 (m ² /year)	α_i^1 (m)	α_l^1 (m)	d_m^2 (m ² /year)	α_i^2 (m)	α_l^2 (m)
Dogger	5×10^{-4}	50	1	5×10^{-4}	50	1
Clay	9.48×10^{-7}	0	0	4.42×10^{-4}	0	0
Limestone	5×10^{-4}	50	1	5×10^{-4}	50	1
Marl	5×10^{-4}	0	0	5×10^{-4}	0	0

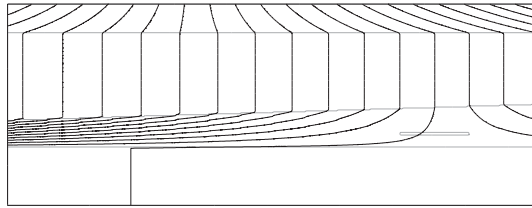


Figure 12. Hydrodynamic load contours for the COUPLEX 1 test case with twenty isovalues between 180 and 340.

We are interested by the elements Iodine ^{129}I and plutonium ^{242}Pu that escape from the repository. In system (6), the iodine is represented by s^1 while the plutonium is depicted by s^2 . The adsorption is assumed linear and is then modelled by two retardation factors R^1 and R^2 in the equations

$$\phi R^k \partial_t c^k + V \cdot \nabla c^k - \text{div}(D^k \nabla c^k) + \phi \lambda^k R^k c^k = f^k(t, x), \quad k = 1, 2$$

The elements generated from the destruction of iodine and plutonium are not taken into account. The other data of this benchmark are summarized in the following:

- In the clay layer, ϕR^1 has the value 0.001 for ^{129}I and 0.2×10^5 for ^{242}Pu . In the other layers, $\phi R^k = 0.1$ for both iodine and plutonium.
- $\lambda^k = \ln 2/T^k$, T^k being the period of the element s^k : $T^1 = 1.57 \times 10^7$ years and $T^2 = 3.76 \times 10^5$ years.
- For the diffusion–dispersion tensor,

$$D^k = d_m^k I + |V|(\alpha_i^k E(V) + \alpha_l^k (I - E(V))), \quad (E(V))_{ij} = \frac{V_i V_j}{|V|^2}$$

and the X -dependent coefficients are given in Table III.

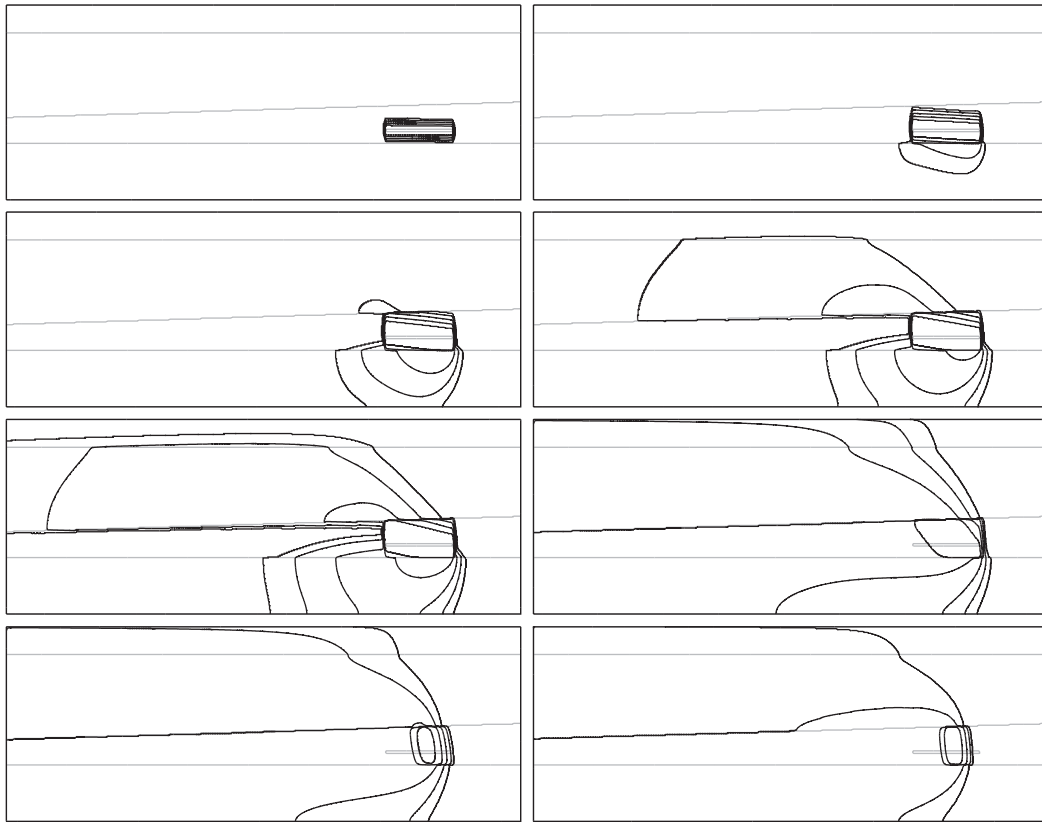


Figure 13. Concentration of ^{129}I from left to right and top to bottom at times 10 110, 50 110, 100 000, 150 000, 200 000, 10^6 , 5×10^6 and 10^7 years. The contour values are 10^{-12} , 10^{-10} , 10^{-8} , 10^{-6} , 10^{-4} .

- The source terms f^k denote the leaked concentrations. They vanish outside the repository and keep constant \bar{f}^k inside. Denoting by S the surface of the repository, the quantities $\tilde{f}^{k,q} = S \bar{f}^{k,q}$ and the times t^q they are related to are given in tabulated form in a data file available on site [4]. Their unity is the mol/year and their appearance is shown on Figure 11.

The initial datum for iodine and plutonium is zero and the boundary conditions are for both

$$\begin{aligned} \frac{\partial c^k}{\partial \mathbf{n}} &= 0 \quad \text{on } \{0\} \times [295.595] \\ \frac{\partial c^k}{\partial \mathbf{n}} &= 0 \quad \text{on } \{0\} \times [0.200] \\ D^k \nabla c^k \cdot \mathbf{n} - c^k V \cdot \mathbf{n} &= 0 \quad \text{on } [0.25000] \times \{0\} \\ c^k &= 0 \quad \text{elsewhere on the boundary} \end{aligned}$$

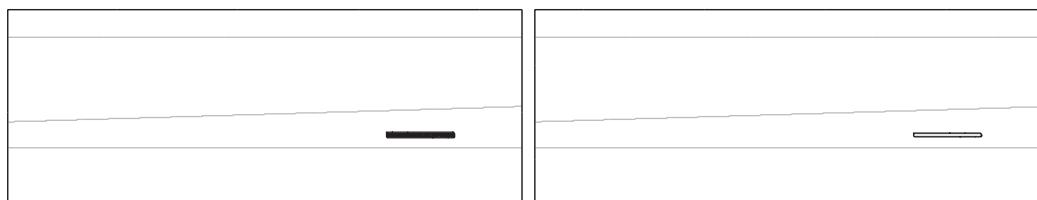


Figure 14. Concentration of ^{242}Pu at times 10^6 years (left), and 5×10^6 years (right). The contour values are 10^{-12} , 10^{-10} , 10^{-8} , 10^{-6} , 10^{-4} .

The hydrodynamic load and concentrations of both radio-elements at time 200, 10110, 50110, 10^6 and 10^7 years are expected.

This benchmark has been performed with the 850×208 uniform Cartesian mesh. The results are drawn on Figures 12–14. We see in Figure 12 that the hydrodynamic load is directly linked to the boundary conditions as the flow goes from right to left in the limestone and dogger, and the frontiers of clay and marl layers are not permeable. The concentrations of iodine are plotted on Figure 13. The effects of the diffusion can be observed everywhere while the convection is only important in limestone and dogger layers and generates a displacement from right to left. The weak retardation phenomenon and the diffusion–dispersion coefficients allow the iodine to exit from the clay layer and its radioactivity period cannot avoid it to move towards the near ground. The concentrations of plutonium are given on Figure 14. The plutonium is more diffusive than the iodine, but its adsorption by the clay rock is so strong that with the same velocity field, its radioactive decay does not allow it to escape from the clay layer until its entire destruction. The results above are in very good agreement with the ones of the literature [2]. This test case highlights the importance of the adsorption phenomenon in the study of miscible displacements in a saturated porous medium.

6. CONCLUSION

In conclusion a stable and robust second-order scheme is built and tested on various test cases. Despite the difficulties involved by the simulation of a real porous medium flow that are the convection phenomenon, the nonlinearity of the adsorption and the strong heterogeneities between the different geological layers a ground is composed with, the approximation yields accurate results. We are able to perform quite realistic simulations of the displacement of radionuclides in porous media. Furthermore, in spite of the slowness of general porous media flows, radionuclides can reach the floor before they are totally destroyed, even if they come from a leak of some containers that are stocked deeply in the underground. This occurs with convenient geological diffusion–dispersion coefficient, and when the adsorption is sufficiently weak, as the displacement of the iodine shows for the COUPLEX 1 benchmark. When the retardation phenomenon is too strong, the radionuclides are trapped in their geological environment. This can be illustrated by the confinement of the plutonium into the clay layer in the same test case.

APPENDIX A: POSITIVITY AND l^∞ STABILITY

In this appendix we adapt some standard results (see References [16, 20]) on the approximation of hyperbolic conservation laws to Equation (12).

Definition 1

A nine points scheme in two space dimensions can be put on the incremental form when for every n there exist twelve real numbers

$$A_{i+\frac{1}{2},j}^1, B_{i-\frac{1}{2},j}^1, A_{i+\frac{1}{2},j+1}^2, B_{i-\frac{1}{2},j+1}^2, A_{i+\frac{1}{2},j-1}^3, B_{i-\frac{1}{2},j-1}^3, D_{i,j+\frac{1}{2}}^1, E_{i,j-\frac{1}{2}}^1, D_{i+1,j+\frac{1}{2}}^2, \\ E_{i+1,j-\frac{1}{2}}^2, D_{i-1,j+\frac{1}{2}}^3, E_{i-1,j-\frac{1}{2}}^3$$

such that

$$G(X_{i,j}, C_{i,j}^{n+1}) = G(X_{i,j}, C_{i,j}^n) \\ + A_{i+\frac{1}{2},j}^1 \Delta C_{i+\frac{1}{2},j}^n - B_{i-\frac{1}{2},j}^1 \Delta C_{i-\frac{1}{2},j}^n + A_{i+\frac{1}{2},j+1}^2 \Delta C_{i+\frac{1}{2},j+1}^n \\ - B_{i-\frac{1}{2},j+1}^2 \Delta C_{i-\frac{1}{2},j+1}^n + A_{i+\frac{1}{2},j-1}^3 \Delta C_{i+\frac{1}{2},j-1}^n - B_{i-\frac{1}{2},j-1}^3 \Delta C_{i-\frac{1}{2},j-1}^n \\ + D_{i,j+\frac{1}{2}}^1 \Delta C_{i,j+\frac{1}{2}}^n - E_{i,j-\frac{1}{2}}^1 \Delta C_{i,j-\frac{1}{2}}^n + D_{i+1,j+\frac{1}{2}}^2 \Delta C_{i+1,j+\frac{1}{2}}^n \\ - E_{i+1,j-\frac{1}{2}}^2 \Delta C_{i+1,j-\frac{1}{2}}^n + D_{i-1,j+\frac{1}{2}}^3 \Delta C_{i-1,j+\frac{1}{2}}^n - E_{i-1,j-\frac{1}{2}}^3 \Delta C_{i-1,j-\frac{1}{2}}^n$$

where

$$\Delta C_{i+\frac{1}{2},j}^n = C_{i+1,j}^n - C_{i,j}^n \quad \text{and} \quad \Delta C_{i,j+\frac{1}{2}}^n = C_{i,j+1}^n - C_{i,j}^n$$

We get the following stability result.

Proposition 3

Assume $C \mapsto G(X, C)$ is an increasing mapping. A scheme on the incremental form in the sense of Definition 1 is l^∞ -stable and positive provided that for every i and j

$$A_{i+\frac{1}{2},j}^1 - D_{i+1,j+\frac{1}{2}}^2 - E_{i+1,j-\frac{1}{2}}^2 \geq 0 \\ D_{i,j+\frac{1}{2}}^1 - A_{i+\frac{1}{2},j+1}^2 - B_{i-\frac{1}{2},j+1}^2 \geq 0 \\ B_{i-\frac{1}{2},j}^1 - D_{i-1,j+\frac{1}{2}}^3 - E_{i-1,j-\frac{1}{2}}^3 \geq 0 \\ E_{i,j-\frac{1}{2}}^1 - B_{i-\frac{1}{2},j-1}^3 - A_{i+\frac{1}{2},j-1}^3 \geq 0 \\ A_{i+\frac{1}{2},j+1}^2 + D_{i+1,j+\frac{1}{2}}^2 \geq 0 \\ D_{i-1,j+\frac{1}{2}}^3 + B_{i-\frac{1}{2},j+1}^2 \geq 0$$

$$\begin{aligned}
 B_{i-\frac{1}{2},j-1}^3 + E_{i-1,j-\frac{1}{2}}^3 &\geq 0 \\
 A_{i+\frac{1}{2},j-1}^3 + E_{i+1,j-\frac{1}{2}}^2 &\geq 0
 \end{aligned}
 \tag{A1}$$

and

$$A_{i+\frac{1}{2},j}^1 + D_{i,j+\frac{1}{2}}^1 + B_{i-\frac{1}{2},j}^1 + E_{i,j-\frac{1}{2}}^1 \leq \theta_{i,j}(G)
 \tag{A2}$$

where

$$\theta_{i,j}(G) = \min \left(\inf_{\substack{z_1, z_2 \in \mathbb{R}_+ \\ z_1 \neq z_2}} \left(\frac{G(X_{i,j}, z_1) - G(X_{i,j}, z_2)}{z_1 - z_2} \right), \inf_{\substack{z_1, z_2 \in \mathbb{R}_- \\ z_1 \neq z_2}} \left(\frac{G(X_{i,j}, z_1) - G(X_{i,j}, z_2)}{z_1 - z_2} \right) \right)$$

Remark

In porous media flow modelling, $C \mapsto G(X, C)$ belongs generally to $\mathcal{C}^1(\mathbb{R}^*; \mathbb{R})$, so that $\theta_{i,j}(G)$ should be replaced by $\inf_{C \in \mathbb{R}^*} (\partial_C G(X_{i,j}, C))$ in (A2). The application $\partial_C G$ is positive.

According to (13), a sufficient CFL-like condition would be

$$A_{i+\frac{1}{2},j}^1 + D_{i,j+\frac{1}{2}}^1 + B_{i-\frac{1}{2},j}^1 + E_{i,j-\frac{1}{2}}^1 \leq \phi(X_{i,j})$$

Proof

We first show the positivity property. Let $C_{i,j}^n \geq 0$, for every i, j . If $C_{i,j}^{n+1} = 0$, there is nothing to show, hence it may be assumed that $C_{i,j}^{n+1} \neq 0$. Taking first $C_{i,j}^n \neq 0$, we define two positive numbers

$$\theta_{i,j}^n = \frac{G(X_{i,j}, C_{i,j}^n)}{C_{i,j}^n} \quad \text{and} \quad \theta_{i,j}^{n+1} = \frac{G(X_{i,j}, C_{i,j}^{n+1})}{C_{i,j}^{n+1}}$$

Scheme (1) becomes

$$\begin{aligned}
 C_{i,j}^{n+1} &= \frac{1}{\theta_{i,j}^{n+1}} (\theta_{i,j}^n - A_{i+\frac{1}{2},j}^1 - D_{i,j+\frac{1}{2}}^1 - B_{i-\frac{1}{2},j}^1 - E_{i,j-\frac{1}{2}}^1) C_{i,j}^n \\
 &\quad + (A_{i+\frac{1}{2},j}^1 - D_{i+1,j+\frac{1}{2}}^2 - E_{i+1,j-\frac{1}{2}}^2) C_{i+1,j}^n + (A_{i+\frac{1}{2},j}^1 - D_{i+1,j+\frac{1}{2}}^2 - E_{i+1,j-\frac{1}{2}}^2) C_{i,j+1}^n \\
 &\quad + (B_{i-\frac{1}{2},j}^1 - D_{i-1,j+\frac{1}{2}}^3 - E_{i-1,j-\frac{1}{2}}^3) C_{i-1,j}^n + (E_{i,j-\frac{1}{2}}^1 - B_{i-\frac{1}{2},j-1}^3 - A_{i+\frac{1}{2},j-1}^3) C_{i,j-1}^n \\
 &\quad + (A_{i+\frac{1}{2},j+1}^2 + D_{i+1,j+\frac{1}{2}}^2) C_{i+1,j+1}^n + (D_{i-1,j+\frac{1}{2}}^3 + B_{i-\frac{1}{2},j+1}^2) C_{i-1,j+1}^n \\
 &\quad + (B_{i-\frac{1}{2},j-1}^3 + E_{i-1,j-\frac{1}{2}}^3) C_{i-1,j-1}^n + (A_{i+\frac{1}{2},j-1}^3 + E_{i+1,j-\frac{1}{2}}^2) C_{i+1,j-1}^n
 \end{aligned}$$

and therefore the assumptions of the proposition yield the positivity of $C_{i,j}^{n+1}$ since $\theta_{i,j}^n \geq \theta_{i,j}(G)$. The proof when $C_{i,j}^n = 0$ is obvious.

Now let us prove the stability property. If $C_{i,j}^{n+1} = C_{i,j}^n$, there is nothing to show. If $C_{i,j}^{n+1} \neq C_{i,j}^n$, we define the positive number

$$\theta_{i,j}^{n+\frac{1}{2}} = \frac{G(X_{i,j}, C_{i,j}^{n+1}) - G(X_{i,j}, C_{i,j}^n)}{C_{i,j}^{n+1} - C_{i,j}^n}$$

Scheme (1) can be rewritten as

$$\begin{aligned} C_{i,j}^{n+1} = & \frac{1}{\theta_{i,j}^{n+\frac{1}{2}}} (\theta_{i,j}^{n+\frac{1}{2}} - A_{i+\frac{1}{2},j}^1 - D_{i,j+\frac{1}{2}}^1 - B_{i-\frac{1}{2},j}^1 - E_{i,j-\frac{1}{2}}^1) C_{i,j}^n \\ & + (A_{i+\frac{1}{2},j}^1 - D_{i+1,j+\frac{1}{2}}^2 - E_{i+1,j-\frac{1}{2}}^2) C_{i+1,j}^n + (D_{i,j+\frac{1}{2}}^1 - A_{i+\frac{1}{2},j+1}^2 - B_{i-\frac{1}{2},j+1}^2) C_{i,j+1}^n \\ & + (B_{i-\frac{1}{2},j}^1 - D_{i-1,j+\frac{1}{2}}^3 - E_{i-1,j-\frac{1}{2}}^3) C_{i-1,j}^n + (E_{i,j-\frac{1}{2}}^1 - B_{i-\frac{1}{2},j-1}^3 - A_{i+\frac{1}{2},j-1}^3) C_{i,j-1}^n \\ & + (A_{i+\frac{1}{2},j+1}^2 + D_{i+1,j+\frac{1}{2}}^2) C_{i+1,j+1}^n + (D_{i-1,j+\frac{1}{2}}^3 + B_{i-\frac{1}{2},j+1}^2) C_{i-1,j+1}^n \\ & + (B_{i-\frac{1}{2},j-1}^3 + E_{i-1,j-\frac{1}{2}}^3) C_{i-1,j-1}^n + (A_{i+\frac{1}{2},j-1}^3 + E_{i+1,j-\frac{1}{2}}^2) C_{i+1,j-1}^n \end{aligned}$$

The scheme being positive, $\theta_{i,j}^{n+\frac{1}{2}} \geq \theta_{i,j}(G)$, and we conclude on the l^∞ -stability since $C_{i,j}^{n+1}$ is a convex combination of the components of the vector C^n . □

APPENDIX B: CONSTRUCTION OF THE LINEARIZED-TRANSPORT-PROJECTION SCHEME (15)

This first-order scheme is based on the Murman finite volume technique. The mapping $C \mapsto G(X, C)$ is assumed differentiable, and the quantity $1/\partial_C G(X, C)$ is denoted by $H(X, C)$. First note that since $\partial_C G$ never vanishes, Equation (12) is equivalent to the simple transport equation

$$\partial_t C + H(X, C) V \cdot \nabla C = 0 \tag{B1}$$

The velocities $u_{i+\frac{1}{2},j}$ and $v_{i,j+\frac{1}{2}}$ are supposed known and constant on every cell sub-domain defined in Figure B1. We set

$$\tilde{V}(X) = \begin{cases} V_{i,j}^1 := (u_{i+\frac{1}{2},j}, v_{i,j+\frac{1}{2}})^T & \text{if } X \in Q_{i,j}^1 \\ V_{i,j}^2 := (u_{i-\frac{1}{2},j}, v_{i,j+\frac{1}{2}})^T & \text{if } X \in Q_{i,j}^2 \\ V_{i,j}^3 := (u_{i-\frac{1}{2},j}, v_{i,j-\frac{1}{2}})^T & \text{if } X \in Q_{i,j}^3 \\ V_{i,j}^4 := (u_{i+\frac{1}{2},j}, v_{i,j+\frac{1}{2}})^T & \text{if } X \in Q_{i,j}^4 \end{cases}$$

The equation

$$\partial_t G(X, C(t, x)) + \tilde{V}(X) \cdot \nabla C(t, X) = 0$$

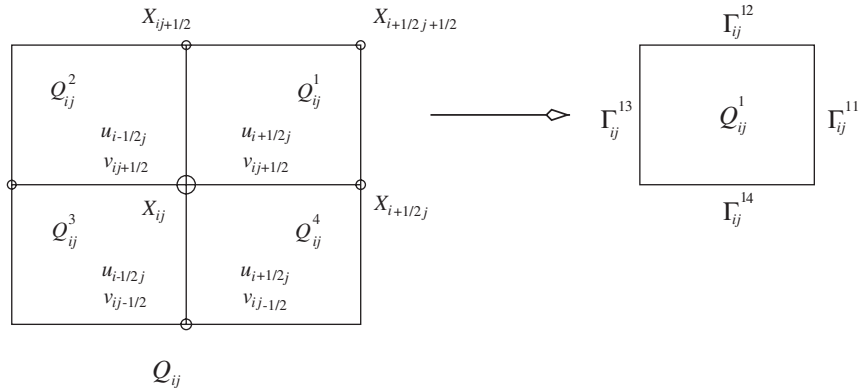


Figure B1. 2D-geometry for the linearized-transport-projection scheme.

is integrated among the space-time cell $(t_n, t_{n+1}) \times Q_{i,j}$. Hence the Stokes formula leads to

$$\begin{aligned} & \int_{Q_{i,j}} (G(X, C(t_{n+1}, X)) - G(X, C(t_n, X))) dX \\ & \int_{t_n}^{t_{n+1}} \int_{\partial Q_{i,j}^1} C(t, X) V_{i,j}^1 \cdot \mathbf{n} dX dt + \int_{t_n}^{t_{n+1}} \int_{\partial Q_{i,j}^2} C(t, X) V_{i,j}^2 \cdot \mathbf{n} dX dt \\ & \int_{t_n}^{t_{n+1}} \int_{\partial Q_{i,j}^3} C(t, X) V_{i,j}^3 \cdot \mathbf{n} dX dt + \int_{t_n}^{t_{n+1}} \int_{\partial Q_{i,j}^4} C(t, X) V_{i,j}^4 \cdot \mathbf{n} dX dt = 0 \end{aligned}$$

where \mathbf{n} stands for the outward unit normal to each sub-cell $\partial Q_{i,j}^l$. To approximate C on $\partial Q_{i,j}^l$, we consider successful Riemann problems on sides $\Gamma_{i,j}^{1,1}$, $\Gamma_{i,j}^{1,2}$, $\Gamma_{i,j}^{1,3}$, $\Gamma_{i,j}^{1,4}$ (see Figure B1). For $\Gamma_{i,j}^{1,1}$, C is evaluated as the exact solution of the constant-velocity convection equation

$$\partial_t \tilde{C}(t, X) + \tilde{H} \tilde{V} \cdot \nabla \tilde{C}(t, X) = 0 \quad \text{for } t \in (t_n, t_{n+1}), X \in Q_{i,j} \tag{B2}$$

where $\tilde{C}(t_n, X)$ is assumed to be known

$$\tilde{C}(t_n, x, y) = \begin{cases} C_{i,j}^n & \text{if } x \leq x_{i+\frac{1}{2}} \text{ and } y \leq y_{j+\frac{1}{2}} \\ C_{i+1,j}^n & \text{if } x > x_{i+\frac{1}{2}} \text{ and } y \leq y_{j+\frac{1}{2}} \\ C_{i+1,j+1}^n & \text{if } x > x_{i+\frac{1}{2}} \text{ and } y > y_{j+\frac{1}{2}} \\ C_{i,j+1}^n & \text{if } x \leq x_{i+\frac{1}{2}} \text{ and } y > y_{j+\frac{1}{2}} \end{cases}$$

and \tilde{H} and \tilde{V} are defined to take into account the direction of the flow

$$\tilde{H} = H_{i+\frac{1}{2},j}^n \quad \text{and} \quad \tilde{V} = \begin{pmatrix} u_{i+\frac{1}{2},j} \\ \tilde{v} \end{pmatrix} \quad \text{with} \quad \tilde{v} = \begin{cases} v_{i,j+\frac{1}{2}} & \text{if } u_{i+\frac{1}{2},j} \geq 0 \\ v_{i+1,j+\frac{1}{2}} & \text{otherwise} \end{cases}$$

The exact solution of (B2) is $\tilde{C}(t, X) = \tilde{C}(t_n, x - \tilde{H}u_{i+\frac{1}{2},j}(t - t_n), y - \tilde{H}\tilde{v}(t - t_n))$.

The same process is repeated on $\Gamma_{i,j}^{1,2}$ with

$$\tilde{H} = H_{i,j+\frac{1}{2}}^n \quad \text{and} \quad \tilde{V} = \begin{pmatrix} \tilde{u} \\ v_{i,j+\frac{1}{2}} \end{pmatrix} \quad \text{with} \quad \tilde{u} = \begin{cases} u_{i+\frac{1}{2},j} & \text{if } v_{i,j+\frac{1}{2}} \geq 0 \\ u_{i+\frac{1}{2},j+1} & \text{otherwise} \end{cases}$$

On $\Gamma_{i,j}^{1,3} \times (t_n, t_{n+1})$ and $\Gamma_{i,j}^{1,4} \times (t_n, t_{n+1})$, we take obviously $\tilde{C} = C_{i,j}^n$. Finally, the same arguments than before for $Q_{i,j}^2$, $Q_{i,j}^3$ and $Q_{i,j}^4$, lead to scheme (15), and Proposition 1 follows easily from Proposition 3.

APPENDIX C: LIMITATION OF SCHEME (16)

A flux limitation technique is used as in Reference [10]. First scheme (16) is written as a perturbation of the linearized transport-projection-like scheme

$$\begin{aligned} G(X_{i,j}, C_{i,j}^{n+1}) &= G_{i,j}^{1,n} \\ &- \frac{v_x}{2} (|u_{i+\frac{1}{2},j}| (\alpha_{ij} - H_{i+\frac{1}{2},j}^n \kappa_{i+\frac{1}{2},j}) \Delta C_{i+\frac{1}{2},j}^n - |u_{i-\frac{1}{2},j}| (\alpha_{ij} - H_{i-\frac{1}{2},j}^n \kappa_{i-\frac{1}{2},j}) \Delta C_{i-\frac{1}{2},j}^n) \\ &- \frac{v_y}{2} (|v_{i,j+\frac{1}{2}}| (\beta_{ij} - H_{i,j+\frac{1}{2}}^n \kappa_{i,j+\frac{1}{2}}) \Delta C_{i,j+\frac{1}{2}}^n - |v_{i,j-\frac{1}{2}}| (\beta_{ij} - H_{i,j-\frac{1}{2}}^n \kappa_{i,j-\frac{1}{2}}) \Delta C_{i,j-\frac{1}{2}}^n) \\ &- \frac{v_x v_y}{4} (H_{i-\frac{1}{2},j}^n u_{i-\frac{1}{2},j}^+ (|v_{i-1,j+\frac{1}{2}}| \Delta C_{i-1,j+\frac{1}{2}}^n - |v_{i-1,j-\frac{1}{2}}| \Delta C_{i-1,j-\frac{1}{2}}^n) \\ &+ H_{i+\frac{1}{2},j}^n u_{i+\frac{1}{2},j}^- (|v_{i+1,j+\frac{1}{2}}| \Delta C_{i+1,j+\frac{1}{2}}^n - |v_{i+1,j-\frac{1}{2}}| \Delta C_{i+1,j-\frac{1}{2}}^n) \\ &+ H_{i,j-\frac{1}{2}}^n v_{i,j-\frac{1}{2}}^+ (|u_{i+\frac{1}{2},j-1}| \Delta C_{i+\frac{1}{2},j-1}^n - |u_{i-\frac{1}{2},j-1}| \Delta C_{i-\frac{1}{2},j-1}^n) \\ &+ H_{i,j+\frac{1}{2}}^n v_{i,j+\frac{1}{2}}^- (|u_{i+\frac{1}{2},j+1}| \Delta C_{i+\frac{1}{2},j+1}^n - |u_{i-\frac{1}{2},j+1}| \Delta C_{i-\frac{1}{2},j+1}^n)) \end{aligned} \quad (C1)$$

where $G_{i,j}^{1,n}$ is defined by (15), $\alpha_{i,j}$ and $\beta_{i,j}$ are defined by (18), and

$$\kappa_{i+\frac{1}{2},j} = v_x |u_{i+\frac{1}{2},j}|, \quad \kappa_{i,j+\frac{1}{2}} = v_y |v_{i,j+\frac{1}{2}}|$$

We obtain the nearly second-order limited scheme (19) thanks to an usual flux limitation argument.

One sets $\sigma_{i+\frac{1}{2},j} = v_x u_{i+\frac{1}{2},j}$ and $\sigma_{i,j+\frac{1}{2}} = v_y v_{i,j+\frac{1}{2}}$. This scheme can be put on the incremental form in the sense of Definition 1 with the corresponding coefficients

$$\begin{aligned}
 A_{i+\frac{1}{2},j}^1 &= \sigma_{i+\frac{1}{2},j}^- \left(\alpha_{i,j} - \frac{1}{2} \left((\alpha_{i,j} - H_{i+\frac{1}{2},j}^n \kappa_{i+\frac{1}{2},j}) \varphi(r_{i+\frac{1}{2},j}^{n-}) \right. \right. \\
 &\quad \left. \left. - (\alpha_{i,j} - H_{i-\frac{1}{2},j}^n \kappa_{i-\frac{1}{2},j}) \frac{\varphi(r_{i-\frac{1}{2},j}^{n-})}{r_{i-\frac{1}{2},j}^{n-}} \right) \right) \\
 B_{i-\frac{1}{2},j}^1 &= \sigma_{i-\frac{1}{2},j}^+ \left(\alpha_{i,j} - \frac{1}{2} \left((\alpha_{i,j} - H_{i-\frac{1}{2},j}^n \kappa_{i-\frac{1}{2},j}) \varphi(r_{i-\frac{1}{2},j}^{n+}) \right. \right. \\
 &\quad \left. \left. - (\alpha_{i,j} - H_{i+\frac{1}{2},j}^n \kappa_{i+\frac{1}{2},j}) \frac{\varphi(r_{i+\frac{1}{2},j}^{n+})}{r_{i+\frac{1}{2},j}^{n+}} \right) \right) \\
 D_{i,j+\frac{1}{2}}^1 &= \sigma_{i,j+\frac{1}{2}}^- \left(\beta_{i,j} - \frac{1}{2} \left((\beta_{i,j} - H_{i,j+\frac{1}{2}}^n \kappa_{i,j+\frac{1}{2}}) \varphi(r_{i,j+\frac{1}{2}}^{n-}) \right. \right. \\
 &\quad \left. \left. - (\beta_{i,j} - H_{i,j-\frac{1}{2}}^n \kappa_{i,j-\frac{1}{2}}) \frac{\varphi(r_{i,j-\frac{1}{2}}^{n-})}{r_{i,j-\frac{1}{2}}^{n-}} \right) \right) \\
 E_{i,j-\frac{1}{2}}^1 &= \sigma_{i,j-\frac{1}{2}}^+ \left(\beta_{i,j} - \frac{1}{2} \left((\beta_{i,j} - H_{i,j-\frac{1}{2}}^n \kappa_{i,j-\frac{1}{2}}) \varphi(r_{i,j-\frac{1}{2}}^{n+}) \right. \right. \\
 &\quad \left. \left. - (\beta_{i,j} - H_{i,j+\frac{1}{2}}^n \kappa_{i,j+\frac{1}{2}}) \frac{\varphi(r_{i,j+\frac{1}{2}}^{n+})}{r_{i,j+\frac{1}{2}}^{n+}} \right) \right) \\
 A_{i+\frac{1}{2},j+1}^2 &= \frac{1}{2} H_{i,j+\frac{1}{2}}^n \sigma_{i,j+\frac{1}{2}}^- \sigma_{i+\frac{1}{2},j+1}^- \left(1 - \frac{1}{2} \left(\varphi(r_{i+\frac{1}{2},j+1}^{n-}) - \frac{\varphi(r_{i-\frac{1}{2},j+1}^{n-})}{r_{i-\frac{1}{2},j+1}^{n-}} \right) \right) \\
 B_{i-\frac{1}{2},j+1}^2 &= \frac{1}{2} H_{i,j+\frac{1}{2}}^n \sigma_{i,j+\frac{1}{2}}^- \sigma_{i-\frac{1}{2},j+1}^+ \left(1 - \frac{1}{2} \left(\varphi(r_{i-\frac{1}{2},j+1}^{n+}) - \frac{\varphi(r_{i+\frac{1}{2},j+1}^{n+})}{r_{i+\frac{1}{2},j+1}^{n+}} \right) \right) \\
 D_{i+1,j+\frac{1}{2}}^2 &= \frac{1}{2} H_{i+\frac{1}{2},j}^n \sigma_{i+\frac{1}{2},j}^- \sigma_{i+1,j+\frac{1}{2}}^- \left(1 - \frac{1}{2} \left(\varphi(r_{i+1,j+\frac{1}{2}}^{n-}) - \frac{\varphi(r_{i+1,j-\frac{1}{2}}^{n-})}{r_{i+1,j-\frac{1}{2}}^{n-}} \right) \right) \\
 E_{i+1,j-\frac{1}{2}}^2 &= \frac{1}{2} H_{i+\frac{1}{2},j}^n \sigma_{i+\frac{1}{2},j}^- \sigma_{i+1,j-\frac{1}{2}}^+ \left(1 - \frac{1}{2} \left(\varphi(r_{i+1,j-\frac{1}{2}}^{n+}) - \frac{\varphi(r_{i+1,j+\frac{1}{2}}^{n+})}{r_{i+1,j+\frac{1}{2}}^{n+}} \right) \right)
 \end{aligned}$$

$$\begin{aligned}
A_{i+\frac{1}{2},j-1}^3 &= \frac{1}{2} H_{i,j-\frac{1}{2}}^n \sigma_{i,j-\frac{1}{2}}^+ \sigma_{i+\frac{1}{2},j-1}^- \left(1 - \frac{1}{2} \left(\varphi(r_{i+\frac{1}{2},j-1}^{n-}) - \frac{\varphi(r_{i-\frac{1}{2},j-1}^{n-})}{r_{i-\frac{1}{2},j-1}^{n-}} \right) \right) \\
B_{i-\frac{1}{2},j-1}^3 &= \frac{1}{2} H_{i,j-\frac{1}{2}}^n \sigma_{i,j-\frac{1}{2}}^+ \sigma_{i-\frac{1}{2},j-1}^+ \left(1 - \frac{1}{2} \left(\varphi(r_{i-\frac{1}{2},j-1}^{n+}) - \frac{\varphi(r_{i+\frac{1}{2},j-1}^{n+})}{r_{i+\frac{1}{2},j-1}^{n+}} \right) \right) \\
D_{i-1,j+\frac{1}{2}}^3 &= \frac{1}{2} H_{i-\frac{1}{2},j}^n \sigma_{i-\frac{1}{2},j}^+ \sigma_{i-1,j+\frac{1}{2}}^- \left(1 - \frac{1}{2} \left(\varphi(r_{i-1,j+\frac{1}{2}}^{n-}) - \frac{\varphi(r_{i-1,j-\frac{1}{2}}^{n-})}{r_{i-1,j-\frac{1}{2}}^{n-}} \right) \right) \\
E_{i-1,j-\frac{1}{2}}^3 &= \frac{1}{2} H_{i-\frac{1}{2},j}^n \sigma_{i-\frac{1}{2},j}^+ \sigma_{i-1,j-\frac{1}{2}}^+ \left(1 - \frac{1}{2} \left(\varphi(r_{i-1,j-\frac{1}{2}}^{n+}) - \frac{\varphi(r_{i-1,j+\frac{1}{2}}^{n+})}{r_{i-1,j+\frac{1}{2}}^{n+}} \right) \right)
\end{aligned}$$

Recall the limiter φ defined by (17) verifies the property

$$\theta_1 > 0, \quad \theta_2 > 0, \quad b \neq 0 \Rightarrow -2\theta_2 \leq \theta_1 \varphi(a) - \theta_2 \frac{\varphi(b)}{b} \leq 2\theta_1$$

If

$$\alpha_{ij} - H_{i\pm\frac{1}{2},j} \kappa_{i\pm\frac{1}{2},j} \geq 0 \quad \text{and} \quad \beta_{i,j} - H_{i,j\pm\frac{1}{2}} \kappa_{i,j\pm\frac{1}{2}} \geq 0 \quad (\text{C2})$$

we get

$$\begin{aligned}
H_{i+\frac{1}{2}}^n \sigma_{i+\frac{1}{2},j}^- \kappa_{i+\frac{1}{2},j} &\leq A_{i+\frac{1}{2},j}^1 \leq \sigma_{i+\frac{1}{2},j}^- (2\alpha_{ij} - H_{i-\frac{1}{2},j}^n \kappa_{i-\frac{1}{2},j}) \\
H_{i-\frac{1}{2}}^n \sigma_{i-\frac{1}{2},j}^+ \kappa_{i-\frac{1}{2},j} &\leq B_{i-\frac{1}{2},j}^1 \leq \sigma_{i-\frac{1}{2},j}^+ (2\alpha_{ij} - H_{i+\frac{1}{2},j}^n \kappa_{i+\frac{1}{2},j}) \\
H_{i,j+\frac{1}{2}} \sigma_{i,j+\frac{1}{2}}^- \kappa_{i,j+\frac{1}{2}} &\leq D_{i,j+\frac{1}{2}}^1 \leq \sigma_{i,j+\frac{1}{2}}^- (2\beta_{i,j} - H_{i,j-\frac{1}{2}}^n \kappa_{i,j-\frac{1}{2}}) \\
H_{i,j+\frac{1}{2}} \sigma_{i,j-\frac{1}{2}}^+ \kappa_{i,j-\frac{1}{2}} &\leq E_{i,j-\frac{1}{2}}^1 \leq \sigma_{i,j-\frac{1}{2}}^+ (2\beta_{i,j} - H_{i,j+\frac{1}{2}}^n \kappa_{i,j+\frac{1}{2}}) \\
0 &\leq A_{i+\frac{1}{2},j+1}^2 \leq H_{i,j+\frac{1}{2}}^n \sigma_{i,j+\frac{1}{2}}^- \sigma_{i+\frac{1}{2},j+1}^- \\
0 &\leq B_{i-\frac{1}{2},j+1}^2 \leq H_{i,j+\frac{1}{2}}^n \sigma_{i,j+\frac{1}{2}}^- \sigma_{i-\frac{1}{2},j+1}^+ \\
0 &\leq D_{i+1,j+\frac{1}{2}}^2 \leq H_{i+\frac{1}{2},j}^n \sigma_{i+\frac{1}{2},j}^- \sigma_{i+1,j+\frac{1}{2}}^- \\
0 &\leq E_{i+1,j-\frac{1}{2}}^2 \leq H_{i+\frac{1}{2},j}^n \sigma_{i+\frac{1}{2},j}^- \sigma_{i+1,j-\frac{1}{2}}^+ \\
0 &\leq A_{i+\frac{1}{2},j-1}^3 \leq H_{i,j-\frac{1}{2}}^n \sigma_{i,j-\frac{1}{2}}^+ \sigma_{i+\frac{1}{2},j-1}^- \\
0 &\leq B_{i-\frac{1}{2},j-1}^3 \leq H_{i,j-\frac{1}{2}}^n \sigma_{i,j-\frac{1}{2}}^+ \sigma_{i-\frac{1}{2},j-1}^+ \\
0 &\leq D_{i-1,j+\frac{1}{2}}^3 \leq H_{i-\frac{1}{2},j}^n \sigma_{i-\frac{1}{2},j}^+ \sigma_{i-1,j+\frac{1}{2}}^- \\
0 &\leq E_{i-1,j-\frac{1}{2}}^3 \leq H_{i-\frac{1}{2},j}^n \sigma_{i-\frac{1}{2},j}^+ \sigma_{i-1,j-\frac{1}{2}}^+
\end{aligned} \quad (\text{C3})$$

so that

$$\begin{aligned}
 A_{i+\frac{1}{2},j}^1 - D_{i+1,j+\frac{1}{2}}^2 - E_{i+1,j-\frac{1}{2}}^2 &\geq \sigma_{i+\frac{1}{2},j}^- H_{i+\frac{1}{2},j}^n (\kappa_{i+\frac{1}{2},j} - (\sigma_{i+1,j-\frac{1}{2}}^+ + \sigma_{i+1,j+\frac{1}{2}}^-)) \\
 D_{i,j+\frac{1}{2}}^1 - A_{i+\frac{1}{2},j+1}^2 - B_{i+1,j+\frac{1}{2}}^2 &\geq \sigma_{i,j+\frac{1}{2}}^- H_{i,j+\frac{1}{2}}^n (\kappa_{i,j+\frac{1}{2}} - (\sigma_{i+\frac{1}{2},j+1}^- + \sigma_{i-\frac{1}{2},j+1}^+)) \\
 B_{i-\frac{1}{2},j}^1 - D_{i-\frac{1}{2},j-1}^3 - E_{i-1,j-\frac{1}{2}}^3 &\geq \sigma_{i-\frac{1}{2},j}^+ H_{i-\frac{1}{2},j}^n (\kappa_{i-\frac{1}{2},j} - (\sigma_{i-1,j-\frac{1}{2}}^+ + \sigma_{i-1,j+\frac{1}{2}}^-)) \\
 E_{i,j-\frac{1}{2}}^1 - A_{i+\frac{1}{2},j-1}^3 - B_{i-1,j+\frac{1}{2}}^3 &\geq \sigma_{i,j-\frac{1}{2}}^+ H_{i,j-\frac{1}{2}}^n (\kappa_{i,j-\frac{1}{2}} - (\sigma_{i-\frac{1}{2},j-1}^+ + \sigma_{i+\frac{1}{2},j-1}^-))
 \end{aligned}$$

To verify the property (A1) in Proposition 3, our choice is to modify some second-order terms: $\kappa_{i+\frac{1}{2},j}$ and $\kappa_{i,j-\frac{1}{2}}$ are, respectively, replaced in (C1) by

$$\begin{aligned}
 \tilde{\kappa}_{i+\frac{1}{2},j} &= \max(\kappa_{i+\frac{1}{2},j}, (\sigma_{i+1,j-\frac{1}{2}}^+ + \sigma_{i+1,j+\frac{1}{2}}^-), (\sigma_{i-1,j-\frac{1}{2}}^+ + \sigma_{i-1,j+\frac{1}{2}}^-)) \\
 \tilde{\kappa}_{i,j+\frac{1}{2}} &= \max(\kappa_{i,j+\frac{1}{2}}, (\sigma_{i+\frac{1}{2},j+1}^- + \sigma_{i-\frac{1}{2},j+1}^+), (\sigma_{i-\frac{1}{2},j-1}^+ + \sigma_{i+\frac{1}{2},j-1}^-))
 \end{aligned}$$

and then assumption (A1) turns to hold. However to justify estimates (C3), the condition (C2) has to be verified with these new coefficients $\tilde{\kappa}_{i+\frac{1}{2},j}$ and $\tilde{\kappa}_{i,j+\frac{1}{2}}$. This is true under the CFL-like conditions (20) and (21). It finally remains to fulfill the assumption (A2) of Proposition 3 to ensure positivity and stability of the scheme. For this, estimations (C3) can be used, and they drive to (22).

ACKNOWLEDGEMENTS

The authors would like to thank Didier Lasseux for fruitful discussions on the model. This research was partially supported by GdR MoMaS (CNRS), France.

REFERENCES

1. Bourgeat A, Gipouloux O, Marusic-Paloka E. Modelling of an underground waste disposal site by upscaling. *Mathematical Methods in the Applied Sciences* 2004; **27**(4):381–403.
2. Bourgeat A, Kern M. Simulation of transport around a nuclear waste disposal site: the COUPLEX test cases. *Computational Geosciences* 2004; **8**(2).
3. Chou CH, Li Q. Characteristics-Galerkin and mixed finite element approximation of contamination by compressible nuclear waste-disposal in porous media. *Numerical Methods for Partial Differential Equations* 1996; **12**(3):315–332.
4. GdR MoMaS Modélisations mathématiques et simulations numériques liées aux problèmes de gestion des déchets nucléaires. <https://mcs.univ-Lyon1.fr/MOMAS/> (28 September 2004).
5. de Marsily G. *Hydrogéologie Quantitative*. Masson: Milan, Italy, 2000.
6. Bear J. *Dynamics of Fluids in Porous Media*. Elsevier: Amsterdam, 1972.
7. Choquet C. Analyse de modèles d'écoulements en milieu poreux hétérogène. *Ph.D. Thesis*, 2002.
8. Choquet C. Radionuclide transport model with wells. *Asymptotic Analysis* 2004; **37**(1):57–78.
9. Kischinhevsky M, Paes-Leme J. Modelling and numerical simulations of contaminant transport in naturally fractured porous media. *Transport in Porous Media* 1997; **26**:25–49.
10. Rasetarinera P. Étude mathématique et numérique de la restauration biologique en milieux poreux. *Ph.D. Thesis*, 1995.

11. Royer P, Auriault JL, Lewandowska J, Serres C. Continuum modeling of contaminant transport in fractured porous media. *Transport in Porous Media* 2002; **49**(3):333–359.
12. Fabrie P, Rasetarinera P. Analyse mathématique d'un système de transport-diffusion-réaction modélisant la restauration biologique d'un milieu poreux. *Revista Matemática de la Universidad Complutense de Madrid* 1996; **9**(2):393–433.
13. Nield DA, Bejan A. *Convection in Porous Media* (2nd edn). Springer: Berlin, 1999.
14. Lanser D, Verwer JG. Analysis of operator splitting for advection–diffusion–reaction problems from air pollution modelling. *Modelling, Analysis and Simulation (MAS)* 1998; **R9805**.
15. Strang G. On the construction and comparison of difference schemes. *SIAM Journal on Numerical Analysis* 1968; **5**:506–517.
16. Godlewski E, Raviart PA. *Hyperbolic Systems of Conservation Laws*, vol. 3. Ellipses: Mathématiques et applications, 1990.
17. Bruneau CH, Fabrie P, Rasetarinera P. An accurate finite difference scheme for solving convection-dominated diffusion equations. *International Journal for Numerical Methods in Fluids* 1997; **24**:169–183.
18. Roe PL. Generalized formulation of TVD Lax–Wendroff schemes. *ICASE Report* 1984; 53–84.
19. Sweby PK. High resolution schemes using flux limiters for hyperbolic conservation laws. *SIAM Journal on Numerical Analysis* 1984; **21**:995–1011.
20. Godlewski E, Raviart PA. *Numerical Approximation of Hyperbolic Systems of Conservation Laws*, vol. 118. Applied Mathematical Sciences, 1995.